IJMMM International Journal of Minerals, Metallurgy and Materials 矿物冶金与材料学报（英文版）

Improvement strategy on thermophysical properties of $A_2B_2O_7$-type rare earth zirconates for thermal barrier coatings applications: A review

Zijian Peng, Yuhao Wang, Shuqi Wang, Junteng Yao, Qingyuan Zhao, Enyu Xie, Guoliang Chen, Zhigang Wang, Zhanguo Liu, Yaming Wang, and Jiahu Ouyang

Cite this article as:
Zijian Peng, Yuhao Wang, Shuqi Wang, Junteng Yao, Qingyuan Zhao, Enyu Xie, Guoliang Chen, Zhigang Wang, Zhanguo Liu, Yaming Wang, and Jiahu Ouyang, Improvement strategy on thermophysical properties of $A_2B_2O_7$-type rare earth zirconates for thermal barrier coatings applications: A review, *Int. J. Miner. Metall. Mater.*, 31(2024), No. 5, pp. 1147-1165. https://doi.org/10.1007/s12613-024-2853-4

View the article online at SpringerLink or IJMMM Webpage.

INTERNATIONAL JOURNAL OF
Minerals, Metallurgy and Materials

Volume 31, Number 5, May 2024
Page 1147

Invited Review

https://doi.org/10.1007/s12613-024-2853-4

Improvement strategy on thermophysical properties of $A_2B_2O_7$-type rare earth zirconates for thermal barrier coatings applications: A review

Zijian Peng[1)], *Yuhao Wang*[1)], *Shuqi Wang*[1)], *Junteng Yao*[1)], *Qingyuan Zhao*[1)], *Enyu Xie*[1)], *Guoliang Chen*[1)], *Zhigang Wang*[2)], *Zhanguo Liu*[1)], *Yaming Wang*[1)], *and Jiahu Ouyang*[1),✉]

1) School of Materials Science and Engineering, Harbin Institute of Technology, Harbin 150001, China
2) School of Materials and Metallurgical Engineering, Inner Mongolia University of Science & Technology, Baotou 014010, China
(Received: 16 October 2023; revised: 16 January 2024; accepted: 14 February 2024)

Abstract: The $A_2B_2O_7$-type rare earth zirconate compounds have been considered as promising candidates for thermal barrier coating (TBC) materials because of their low sintering rate, improved phase stability, and reduced thermal conductivity in contrast with the currently used yttria-partially stabilized zirconia (YSZ) in high operating temperature environments. This review summarizes the recent progress on rare earth zirconates for TBCs that insulate high-temperature gas from hot-section components in gas turbines. Based on the first principles, molecular dynamics, and new data-driven calculation approaches, doping and high-entropy strategies have now been adopted in advanced TBC materials design. In this paper, the solid-state heat transfer mechanism of TBCs is explained from two aspects, including heat conduction over the full operating temperature range and thermal radiation at medium and high temperature. This paper also provides new insights into design considerations of adaptive TBC materials, and the challenges and potential breakthroughs are further highlighted for extreme environmental applications. Strategies for improving thermophysical performance are proposed in two approaches: defect engineering and material compositing.

Keywords: rare earth zirconates; thermal barrier coatings; defect engineering; doping and compositing; thermal conductivity; thermal expansion

1. Introduction

The employment of gas turbine engines is prevalent in the fields of power generation, aviation, and astronautics [1–2]. With the growing demand for gas turbine efficiency, high-performance nickel-based superalloys have been developed rapidly by adding rare metallic elements and exploiting single-crystal manufacturing technology. Despite advancing to its fifth generation, the superalloy is still faced with inherent limitations such as reduced strength and inadequate corrosion resistance at elevated temperature, rendering it susceptible to failure when exposed to temperature exceeding 1473 K for extended periods. In the 1990s, researchers began to focus on developing and manufacturing ceramic thermal barrier coatings (TBCs) because traditional turbine materials had attained their maximum temperature capabilities. The deposition of TBCs is a common practice in high-temperature components of gas turbines and other propulsion systems, aimed at protecting the underlying superalloy substrates and enabling engines to achieve enhanced efficiency even in elevated temperature [1–5].

The use of advanced TBCs enhanced gas temperature and reduced substrate temperature through the heat transfer facilitated by the flow of cooling air, thereby optimizing engine efficiency. To achieve the above objective, TBC materials can be selected on the basis of the following criteria: (1) possessing a high melting point, (2) exhibiting low thermal conductivity, (3) exhibiting chemical inertness, (4) displaying high thermal expansion to match the superalloy substrate, (5) maintaining high phase stability between room temperature and the operating temperature, and (6) providing good sintering resistance. The standard TBC system comprises four stages of coating such as ceramic topcoat (TC), thermally grown oxide layer (TGO), bond coat (BC), superalloy base material (BM), and substrate (SUB) [6–7]. The topcoat TBC materials with 250 μm in thickness can reduce surface temperature by ~150°C and are generally deposited through various techniques, such as atmospheric plasma spraying (APS) and electron beam–physical vapor deposition (EB-PVD) [2,8].

The commonly used ceramic material for TBCs is typically composed of 7wt%–8wt% yttria-stabilized zirconia (YSZ), which exhibits relatively low thermal conductivity and unique comprehensive mechanical properties [1,5–7]. However, a higher gas temperature in advanced engines has recently been in demand. The combustion chamber temper-

✉ Corresponding author: Jiahu Ouyang E-mail: ouyangjh@hit.edu.cn

ature of a gas engine must be elevated to 1300–1700°C to achieve an enhanced thrust–weight ratio. Under these conditions of service, YSZ is restricted to future applications above 1200°C because of a series of problems, such as TGO thickening, nonequilibrium phase transformation, and hot corrosion from silicate melts generally known as CMAS [4,9]. The $A_2B_2O_7$-type compounds of pyrochlore-type and fluorite-type rare earth zirconates have been considered as promising candidates for next-generation gas turbine TBCs due to their lower sintering rate, better phase stability within the temperature range from room temperature to the melting point, and lower thermal conductivity than YSZ. These characteristics are crucial for ensuring the optimal performance of gas turbine components under high-temperature operating conditions. However, the limitations on the thermal expansion coefficient (TEC) and inadequate damage tolerance remain the primary obstacles to further application of rare earth zirconates [9–12]. The mechanical and thermophysical properties of typical ceramics suitable for use in TBC systems are summarized in Table 1.

Table 1. Mechanical and thermophysical properties of typical TBC materials

Materials	Young's modulus, E / GPa	Poisson's number, ν	Thermal conductivity, λ / ($W \cdot m^{-1} \cdot K^{-1}$)	Thermal expansion coefficient, α / (10^{-6} K^{-1})	Heat capacity, C_p / ($J \cdot g^{-1} \cdot K^{-1}$)	Refs.
$La_2Zr_2O_7$	175 (293 K)	—	1.15 (1723 K)	9.1 (1273 K)	0.49 (1273 K)	[10,13–14]
$Sm_2Zr_2O_7$	—	—	1.21 (1473 K)	11.3 (1473 K)	—	[15]
$BaZrO_3$	181 (293 K)	—	3.42 (1273 K)	8.1 (1273 K)	0.45 (1273 K)	[10]
Al_2O_3	30 (293 K)	0.26 (293 K)	5.8 (1400 K)	9.6 (1273 K)	—	[9,13]
Garnet ($Y_3Al_5O_{12}$)	—	—	3.0 (1273 K)	9.1 (1273 K)	—	[16]
Lanthanum aluminate ($LaMgAl_{11}O_{19}$)	—	—	1.7 (1273 K)	10.1 (1473 K)	0.86 (1273 K)	[17–18]
$ErTaO_4$	128 (293 K)	0.33 (293 K)	1.6 (1173 K)	10.7 (1473 K)	—	[19]
Eu_3TaO_7	245 (293 K)	0.27 (293 K)	1.54 (1173 K)	9.8 (1473 K)	0.42 (1173 K)	[20]
Dy_3NbO_7	235 (293K)	—	—	10.6 (1273K)	—	[21]
Gd_3NbO_7	211 (293K)	—	1.4 (1273 K)	10.4 (1673K)	—	[22]
$LaPO_4$	133 (293 K)	0.28 (293 K)	1.8 (973 K)	10.5 (1273 K)	—	[23]
8YSZ coating	40 (293 K)	0.22 (293 K)	—	10.7 (1273 K)	—	[24]
NiCoCrAlY (bond coat of TBC)	86 (293 K)	0.3 (293 K)	—	17.5 (1273 K)	—	[24]
IN738 superalloy	197 (293 K)	0.3 (293 K)	—	16 (1273 K)	—	[24]

The application of density functional theory (DFT) based on the first principles calculation method has gained considerable attention in the field of materials science. DFT relies on solving the Kohn–Sham equation to accurately determine the structural properties of materials and, subsequently, the thermophysical properties. Much effort has been directed at rare earth zirconates for nearly 20 years, focusing on thermal conductivity and TEC from the theoretical foundation to high-entropy design [12,25–30]. This paper presents solid-state heat transfer mechanisms and thermophysical performance enhancement strategies based on defect engineering and the material compositing approach. In addition, recent progress on the intrinsic thermophysical properties of rare earth zirconate TBC materials has been reviewed, and future considerations on the materials design of rare earth zirconates are highlighted.

2. Heat transfer mechanism in rare earth zirconates

The dominant mechanism of heat conduction in rare earth zirconates is generally considered the propagation of phonons [31]. According to the Debye model, the thermal conductivity (κ) of ceramic materials can be depicted as follows [32]:

$$\kappa = \frac{1}{3}\int_{\omega} C_V v_s l \mathrm{d}\omega \tag{1}$$

where C_V represents the specific heat, v_s denotes the average sound velocity, ω signifies the phonon frequency, and l corresponds to the phonon mean free path. Notably, regulating the phonon mean free path emerges as a feasible approach.

In solid materials, the presence of defects, boundaries, and other phonon scattering effects in a lattice structure restricts the mean free path of phonons and the overall thermal conductivity [33]. On the basis of the assumption that all phonon scattering processes can be effectively represented by relaxation times (τ_C), Callaway formulated an expression for thermal conductivity as [24]

$$\kappa = \frac{k_B}{2\pi^2 v_s}\left(\frac{k_B T}{\hbar}\right)^3 \int_0^{\theta_D/T} \tau_C(x)\frac{x^4 e^x}{(e^x-1)^2}\mathrm{d}x \tag{2}$$

where $x = \hbar\omega/(k_B T)$, k_B denotes the Boltzmann constant, $\hbar$ represents the reduced Planck constant, T is the temperature, and θ_D signifies the Debye temperature. Then, the combined relaxation time τ_C is defined as [34]

$$\tau_C^{-1} = \tau_P^{-1} + \tau_D^{-1} + \tau_B^{-1} \tag{3}$$

where τ_P, τ_D, and τ_B are denoted as the relaxation time of phonon–phonon scattering, phonon–defect scattering, and phonon–boundary scattering, respectively.

In practical materials, phonon–boundary scattering can be

neglected throughout the temperature range. For phonon–point defect scattering, point defects contribute to the inverse relaxation time, Klemens [35] proposed the following expressions:

$$\tau_D^{-1} = A\omega^4 \tag{4}$$

If point defects scatter mainly in virtue of their mass difference, the coefficient A of the above formula (4) can be expressed as

$$A = \frac{\Omega\Gamma}{4\pi v_s^3} \tag{5}$$

where ω corresponds to the phonon frequency, Ω is the average volume per atom, and Γ represents the phonon scattering coefficient.

Furthermore, phonon–phonon scattering (Umklapp scattering) can be presented in terms of its relaxation time, illustrated as

$$\tau_P^{-1} = B\omega^2 \tag{6}$$

When $T > \theta_D$, $B \propto T$, and C represents the proportionality constant:

$$B = CT \tag{7}$$

Therefore, the thermal conductivity of materials can be transformed from Eq. (1) as [36]

$$\kappa = \frac{k_B}{2\pi^2 v_s \sqrt{(ACT)}} \tan^{-1}\left[\frac{k_B\theta_D}{\hbar}\left(\frac{A}{CT}\right)^{\frac{1}{2}}\right] \tag{8}$$

The thermal conductivity can be deduced from Eq. (8), indicating that phonon–phonon scattering results in a temperature-dependent inverse relationship with thermal conductivity. In addition, the thermal conductivity of materials with defects is inversely proportional to the square root of the coefficient for phonon scattering.

Above 600°C, rare earth zirconates exhibit infrared transparency. High-temperature gas produces intense infrared radiation, which can penetrate the material and transfer heat directly to the substrate, finally leading to a reduction in the thermal barrier effect of rare earth zirconates at gas turbine operation temperature. Consequently, the high-emissivity design of rare earth zirconates appears particularly important. According to Kirchhoff's law, the emissivity of a body at equilibrium at a given wavelength λ and temperature T is equal to its absorption coefficient. The emissivity, denoted as ε, is defined as the ratio of energy radiated by a material to that radiated by a black body (a body that absorbs all incident radiation and emits all absorbed energy with the same spectrum $\varepsilon = 1$), which is described by Eq. (9) [37]:

$$\varepsilon(T) = \frac{E(T)}{E_b(T)} \tag{9}$$

where $E(T)$ represents the radiant heat of gray body to its surroundings at temperature T, and $E_b(T)$ corresponds to the radiant heat of a black body to its surroundings at temperature T. The closer the emissivity value is to 1, the stronger the ability of an object to radiate electromagnetic waves [38]. Therefore, the higher the emissivity of an object in the infrared band, the more heat it radiates to outer space, the higher the heat dissipation power, and the faster the cooling [39].

The infrared radiation of a material is mainly affected by its internal structure, which mainly includes two mechanisms: electronic transitions and lattice vibrations [40–41]. Depending on the activation energy required, an electron transition corresponds to infrared absorption in the short band of 0.76–8 μm, while a lattice vibration corresponds to infrared absorption in the long band of 8–25 μm [42]. The material radiates infrared electromagnetic waves because the electrons of internal atomic, molecular, and ionic systems transition between energy levels and the dipole moment change induced by molecular bond vibrations [43].

3. Strategy for improving thermophysical performance

3.1. Defect engineering

3.1.1. Pure phase single rare earth zirconates

$Ln_2Zr_2O_7$ (Ln = lanthanide series rare-earth elements) with a pyrochlore or fluorite structure contains approximately 12.5% (1/8) intrinsic oxygen vacancies, which generates a low thermal conductivity. Pyrochlore-type $Ln_2Zr_2O_7$ with an ordered structure can be regarded as $A_2B_2O_6O'$, whose crystalline sites 16c, 16d, 48f, 8a, and 8b are occupied by the A, B, O, O' ions and oxygen vacancies, respectively. In contrast, fluorite-type $Ln_2Zr_2O_7$ has totally disordered cations, for which it can be regarded as AO_2 with one-eighth intrinsic oxygen vacancies [44]. Fig. 1 shows the simulated models of the pyrochlore and defective fluorite structures of rare earth zirconates.

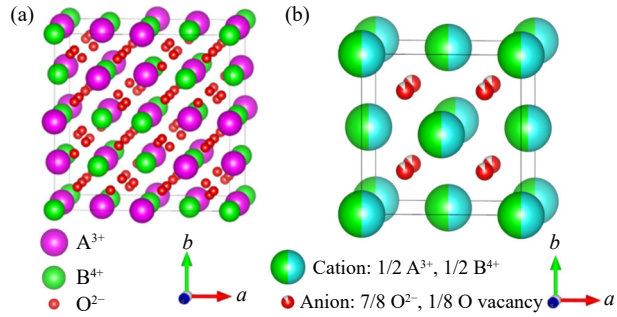

Fig. 1. Simulated models of crystal structures of rare earth zirconates: (a) pyrochlore; (b) defective fluorite.

The thermophysical properties of $Ln_2Zr_2O_7$ rare earth zirconates synthesized by various methods have been extensively investigated by numerous scholars. The current consensus is that an emphasis should be placed on investigating the thermal conductivity (Fig. 2) and TEC (Fig. 3) of $Ln_2Zr_2O_7$ at high temperature (the maximum test temperature varies across different sources of references) as the service temperature increases. The thermophysical characteristics of identical ceramics can vary substantially, which can be attributed to the differences in the experimental design and particle size of raw materials. Nonetheless, the thermal conductivity of $Ln_2Zr_2O_7$ is considerably lower than that of YSZ; however, more efforts are needed to enhance the TEC to im-

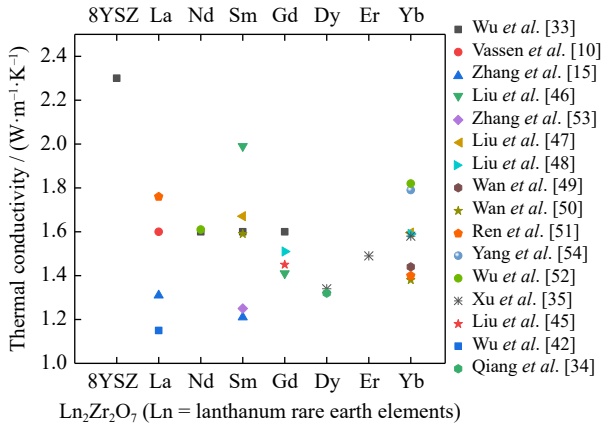

Fig. 2. Thermal conductivity of $Ln_2Zr_2O_7$ at the maximum test temperature varies across different sources of references.

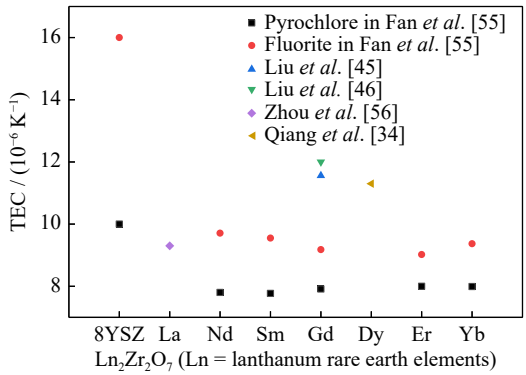

Fig. 3. Thermal expansion coefficient of $Ln_2Zr_2O_7$ at the maximum test temperature varies across different sources of references.

prove the thermal cycling life.

(1) $Ln_2Zr_2O_7$ bulk materials.

Wu *et al.* [57] measured the thermal conductivities of hot-pressed $Ln_2Zr_2O_7$ (Ln = Gd, Sm, and Nd) ceramics compared with pressureless-sintered 7wt% yttria-stabilized zirconia (7YSZ). The measured thermal conductivities of all rare earth zirconates were nearly identical, exhibiting a 30% decrease compared to that of 7YSZ at 25–700°C. $Dy_2Zr_2O_7$ with a defective fluorite structure was prepared by Xu *et al.* [58] through a solid-state reaction at 1600°C for 10 h. The TEC of the $Dy_2Zr_2O_7$ ceramic (11.3×10^{-6} °C^{-1}, at 1300°C) was slightly higher than that of conventional 8wt% Y_2O_3–ZrO_2 (8YSZ), while its thermal conductivity (1.32 W/(m·K), at 800°C) was distinctly lower than that of 8YSZ. Defective fluorite-type $Ln_2Zr_2O_7$ (Ln = Dy, Er, and Yb) with similar oxygen vacancy concentrations, approximately 12.5% (1/8), have considerably lower thermal conductivities of approximately 1.3–1.9 W/(m·K) than the referenced pyrochlore-type $Ln_2Zr_2O_7$ ceramics at 20–800°C [59].

Furthermore, a combination of first-principles calculations and the quasi-harmonic (QH) approximation is adopted by Feng *et al.* [60] to predict the thermal conductivities of rare earth zirconates with a pyrochlore structure. The thermal conductivities are estimated under Slack's model, which agrees with experimental results. Another consideration for the first-principles calculations is DFT with a plane-wave pseudopotential total energy scheme method by Yang *et al.* [61], a new approach to studying the electronic structure and mechanical and thermal properties of $La_2B_2O_7$ (B = Zr, Sn, Hf, and Ge) pyrochlore (Fig. 4). In addition, the first-principles with QH phonon calculations can also be applied to predict the coefficient of thermal expansion. Lan *et al.* [62] proposed a QH approximation approach based on stable phonon modes and further clarified that the QH Debye model overestimated the observed TECs of $RE_2Zr_2O_7$ pyrochlores. However, a more reliable method is still urgently needed to characterize the thermal expansion property. A model proposed by Wang *et al.* [63] integrated Grüneisen's equation and the Debye heat capacity model to establish an efficient coupled model of α_∞, which characterizes the coefficient of thermal expansion at extremely high temperatures. The α_∞ values of cubic ZrO_2, cubic HfO_2, $La_2Zr_2O_7$, $Pr_2Zr_2O_7$, $Gd_2Zr_2O_7$, and $Dy_2Zr_2O_7$ were calculated, which exhibited a similar trend to the measured experimental results. Chen *et al.* [64] studied the influence of the concentration of cation vacancies on TEC by constructing nonstoichiometric gadolinium zirconate using first-principles calculations. Excessive Gd^{3+} increases the TEC of ceramics from 11.108×10^{-6} to 11.593×10^{-6} K^{-1}. Therefore, a high TEC of $Gd_2Zr_2O_7$ ceramics can be achieved by introducing excessive Gd^{3+} because of the increased disorder in Gd–O bonds, enhanced thermal diffusivity, and reduced solid solubility.

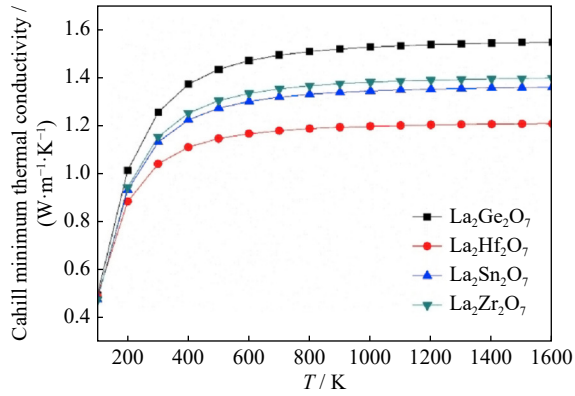

Fig. 4. Thermal conductivity of $La_2B_2O_7$ (B = Zr, Sn, Hf, and Ge) pyrochlore vs. temperature according to Cahill's model. Reprinted from *J. Alloys Compd.*, 663, J. Yang, M. Shahid, M. Zhao, J. Feng, C. Wan, and W. Pan, Physical properties of $La_2B_2O_7$ (B = Zr, Sn, Hf, and Ge) pyrochlore: First-principles calculations, 834, Copyright 2016, with permission from Elsevier.

In addition to the solid-state reaction and chemical coprecipitation methods, soft chemical processes using alkoxide and citrate synthesis can be performed at a relatively low temperature to synthesize rare earth zirconates ($RE_2Zr_2O_7$, RE = La and Gd) [65]. Xu *et al.* [14] proposed a co-ions complexation method (CCM) to synthesize pyrochlore lanthanum zirconate at 1300°C. The grain size of $La_2Zr_2O_7$ is approximately 300 nm, which may lead to a lower thermal conductivity of 1.15 W/(m·K) (at 1450°C) compared to 1.99 W/(m·K) by the solid-state method. A

schematic of the complexation and crystallization in CCM is shown in Fig. 5.

Kaliyaperumal *et al*. [66] studied phase transformation from pyrochlore to fluorite in nanocrystalline $Nd_2Zr_2O_7$, which is accomplished at 1300°C (Fig. 6). Despite the same concentration of oxygen vacancies, the structural transition from pyrochlore to fluorite occurring in rare earth zirconate remains an important factor affecting TBC applications.

(2) $Ln_2Zr_2O_7$ coating materials.

In addition to bulk materials, rare earth zirconates with intrinsic oxygen vacancies as the ceramic topcoat have attracted considerable attention. Zhao *et al*. [67] investigated $Sm_2Zr_2O_7$ coatings using electron beam evaporation and directed vapor deposition (EB-DVD, Fig. 7). Because of the vapor-phase disparities of the constituent oxides, the cation ordering necessary for pyrochlore structure formation is impeded by kinetic constraints, ultimately resulting in an equilibrium pyrochlore structure in the as-deposited $Sm_2Zr_2O_7$ with thermal conductivity of (0.5 ± 0.1) W/(m·K) at 1100°C. Yu *et al*. [68] compared the plasma-sprayed $Sm_2Zr_2O_7$ coat-

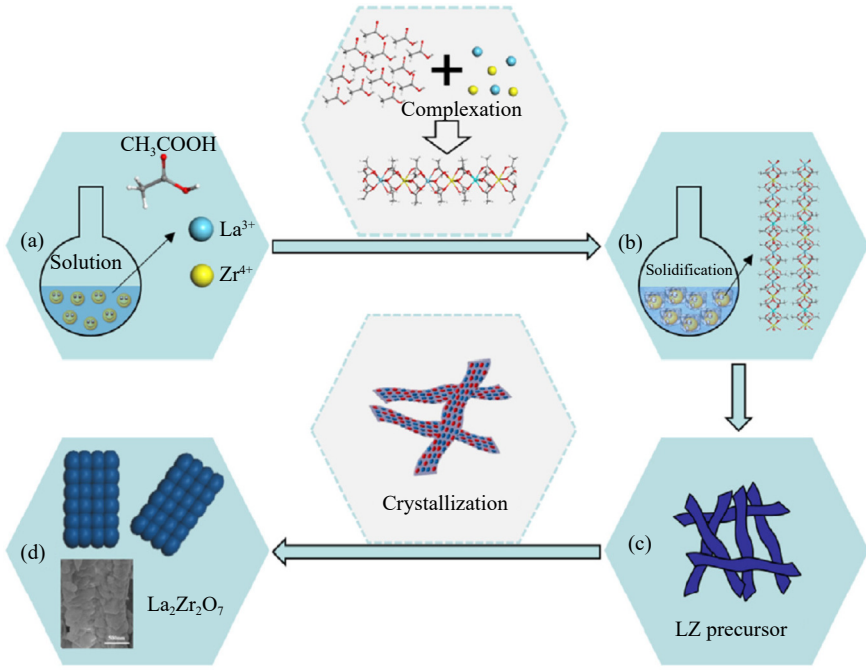

Fig. 5. Schematic of the complexation and crystallization in CCM. Reprinted from *J. Eur. Ceram. Soc.*, 37, C. Xu, H. Jin, Q. Zhang, *et al.*, A novel Co-ions complexation method to synthesize pyrochlore $La_2Zr_2O_7$, 2871, Copyright 2017, with permission from Elsevier (LZ represents $La_2Zr_2O_7$).

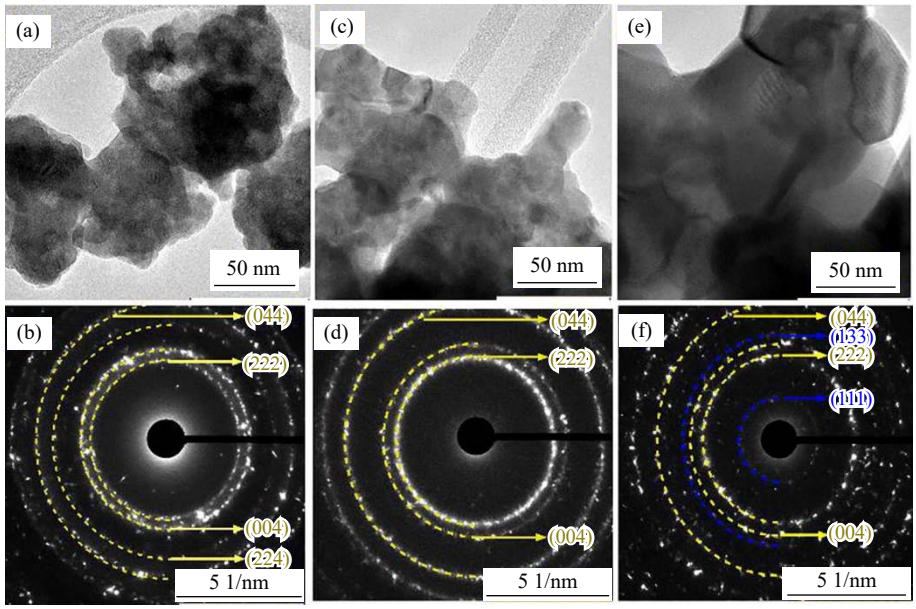

Fig. 6. TEM images and SAED patterns of $Nd_2Zr_2O_7$ heat treated at (a, b) 800°C, (c, d), 1000°C, and (e, f) 1300°C. Reprinted from *Mater. Lett.*, 228, C. Kaliyaperumal, A. Sankarakumar, J. Palanisamy, and T. Paramasivam, Fluorite to pyrochlore phase transformation in nanocrystalline $Nd_2Zr_2O_7$, 493, Copyright 2018, with permission from Elsevier.

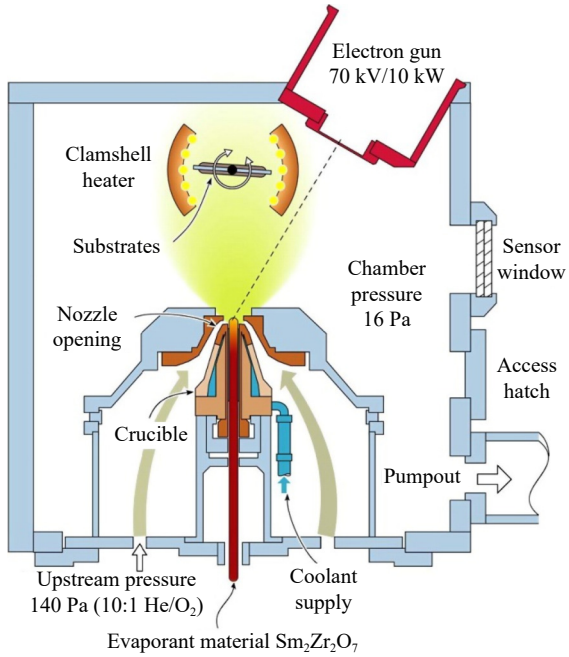

Fig. 7. Schematic of the directed vapor deposition (DVD) apparatus used to deposit $Sm_2Zr_2O_7$ coatings. Reprinted from *Surf. Coat. Technol.*, 203, H. Zhao, C. G. Levi, and H.N.G. Wadley, Vapor deposited samarium zirconate thermal barrier coatings, 3157, Copyright 2009, with permission from Elsevier.

ings with plasma-sprayed 8YSZ, as shown in Fig. 8. $Sm_2Zr_2O_7$ coatings exhibited a lower thermal conductivity than 8YSZ because of thin individual splats. Because of rapid cooling, the defective fluorite phase in the as-sprayed $Sm_2Zr_2O_7$ coating can transform into the pyrochlore structure during heat treatment above 1200°C. Zhao *et al*. [69] deposited $Sm_2Zr_2O_7$ and $Sm_2Zr_2O_7$/YSZ double-layer ceramic coatings on a polished NiCoCrAlY bond coat using the electron beam–physical vapor deposition method. The YSZ layer in the double-layer coatings serves as a diffusion barrier, resulting in a reduced TGO growth rate and extended lifespan. In addition, a new solution combustion process for synthesizing plasma sprayable $La_2Zr_2O_7$ powders after granulation was reported by Aruna *et al*. [70]. Plasma-sprayed $La_2Zr_2O_7$ coatings exhibited a thermal conductivity of 1.08 W/(m·K) at 900°C. Furthermore, a double-layer $Gd_2Zr_2O_7$/YSZ TBC topcoat was deposited via a solution precursor plasma spray process (SPPS) by Jiang *et al*. [71]. The double-layer $Gd_2Zr_2O_7$/YSZ coatings had thermal cyclic durability comparable to single-layer SPPS YSZ coating, which stabilized the phase/microstructure under the integrated gasification combined thermal cycling (IGCC) environment up to 300 h. Moreover, Mahade *et al*. [72] studied a multilayered $Gd_2Zr_2O_7$/YSZ TBC approach via suspension plasma spraying, which exhibited a low thermal conductivity and improved thermal cyclic lifespan; the SEM micrographs of multilayered $Gd_2Zr_2O_7$/YSZ TBCs are shown in Fig. 9.

In summary, doping with rare earth oxides into zirconia or $A_2B_2O_7$-type zirconates is used to tailor the concentration of oxygen vacancies and the ordering degree of rare earth zirconates, which is directly correlated with thermal conductivity and thermal expansion property. Although the adjustment in the concentration of oxygen vacancies is specifically tough

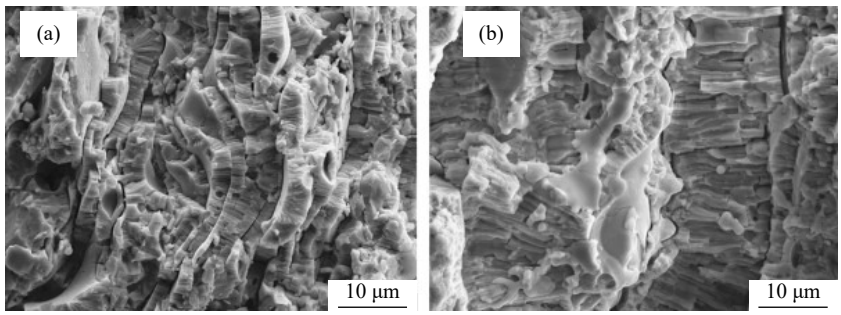

Fig. 8. SEM micrographs of the fracture surface of (a) $Sm_2Zr_2O_7$ and (b) 8YSZ coatings. Reprinted from *J. Eur. Ceram. Soc.*, 30, J. Yu, H. Zhao, S. Tao, X. Zhou, and C. Ding, Thermal conductivity of plasma-sprayed $Sm_2Zr_2O_7$ coatings, 799, Copyright 2010, with permission from Elsevier.

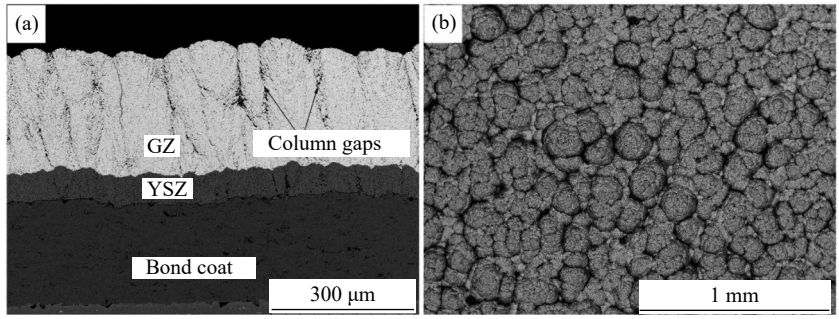

Fig. 9. SEM micrographs of the as-sprayed double-layer $Gd_2Zr_2O_7$/YSZ TBC: (a) cross section and (b) top surface morphology. Reprinted from *Surf. Coat. Technol.*, 283, S. Mahade, N. Curry, S. Björklund, N. Markocsan, and P. Nylén, Thermal conductivity and thermal cyclic fatigue of multilayered $Gd_2Zr_2O_7$/YSZ thermal barrier coatings processed by suspension plasma spray, 329, Copyright 2015, with permission from Elsevier.

[11], the abovementioned literature laid the foundation of defect engineering for rare earth zirconates.

3.1.2. Substitutions

Rare earth zirconates are characterized by a high concentration of intrinsic oxygen vacancies, which are difficult to enhance and even facilitate the diffusion of oxygen, thereby promoting the growth of TGO [73]. The substitution method is an alternative approach to reducing the phonon mean free path while maintaining the intrinsic concentration of vacancies unchanged. Equivalent substitutions of trivalent rare-earth elements at the A site or tetravalent cations at the Zr site represent great chemical and structural compatibility and flexibility, with even infinite solution concentration compared to the fixed concentration of the intrinsic concentration of vacancies. In addition, substitutions of elements with different cationic radii can easily lead to lattice distortions in the pyrochlore or fluorite structure, which can be effectively used to reduce thermal conductivity. According to these characteristics, various doped rare earth zirconates have been developed over the decades.

(1) A-site doping.

A site doping is endowed with a wealth of options due to the diverse range of rare earth elements available. Since the onset of the 21st century, extensive research has been conducted on A site doping in rare earth zirconates. Lehmann *et al*. [74] investigated the thermal conductivities and TECs of lanthanum zirconates doped with and without partial or complete substitutions (Fig. 10). The thermal conductivities of the modified lanthanum zirconates are lower than that of pure lanthanum zirconate, and complete substitution of the lanthanum by neodymium, europium, and gadolinium causes an evident increase in TECs. Liu *et al*. [75] investigated the thermophysical properties of $Nd_xZr_{1-x}O_{2-x/2}$ (x = 0.1, 0.2, 0.3, 0.4, 0.5) ceramics synthesized using chemical coprecipitation and the calcination method. A low thermal conductivity of 1.50–2.01 W/(m·K) was obtained from room temperature to 1400°C. Furthermore, Liu *et al*. [45] prepared $(Nd_xGd_{1-x})_2Zr_2O_7$ (x = 0, 0.1, 0.3, 0.5, 0.7, 0.9, 1.0) ceramics to investigate the thermal conductivity and thermal expansion property. The thermal conductivity decreases from room temperature to approximately 800°C and then increases because of the influence of high-temperature infrared radiation. The reduction of TEC is attributed to an increase in Nd content.

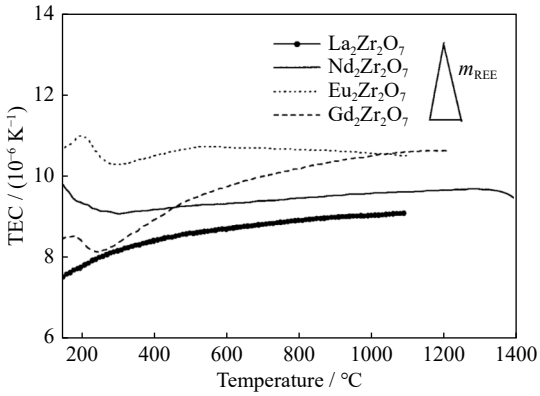

Fig. 10. Thermal expansion coefficients versus the temperature of completely substituted and pure lanthanum zirconates. H. Lehmann, D. Pitzer, G. Pracht, R. Vassen, and D. Stöver, *J. Am. Ceram. Soc.*, 86, 1338(2004) [74]. Copyright Wiley-VCH Verlag GmbH & Co. KGaA. Reproduced with permission.

The structural evolution and thermophysical properties of $(Sm_xGd_{1-x})_2Zr_2O_7$ ($0 \le x \le 1.0$) were reported by Liu *et al*. [46] via a chemical coprecipitation and calcination method. The measured thermal conductivities are 1.20–1.99 W/(m·K), with a slight increase above 800°C. A similar tendency was observed in $(Yb_xSm_{1-x})_2Zr_2O_7$ ($0 \le x \le 1.0$) ceramics and $(Yb_xGd_{1-x})_2Zr_2O_7$ ($0 \le x \le 1.0$) ceramics by Liu *et al*. [47–48]. Additionally, a glass-like thermal conductivity in $(La_{1-x}Yb_x)_2Zr_2O_7$ ($1/6 \le x \le 1/3$), as shown in Fig. 11, and the large atomic displacement parameter of the Yb^{3+} impurity was observed by Wan *et al*. [49], which illustrates that resonant scattering by the rattling Yb^{3+} is mainly responsible for the glass-like thermal conductivity. Wan *et al*. [50] investigated the order–disorder transition in $(Sm_{1-x}Yb_x)_2Zr_2O_7$ ceramics as a function of composition parameter x. A discontinuous phase transition from an ordered pyrochlore phase to a disordered defective fluorite phase is found within the compositional range of x = 1/6 to x = 1/3, in which a minimum thermal conductivity is located at a transition composition of $(Sm_{2/3}Yb_{1/3})_2Zr_2O_7$.

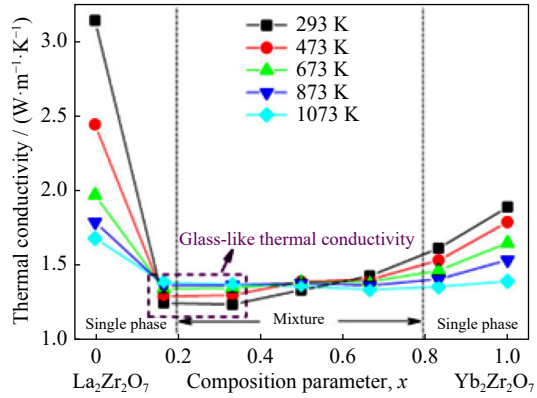

Fig. 11. Glass-like thermal conductivities of $(La_{1-x}Yb_x)_2Zr_2O_7$ (x = 0, 1/6, 1/3, 1/2, 2/3, 5/6, 1). Reprinted from *Acta Mater.*, 58, C. Wan, W. Zhang, Y. Wang, *et al.*, Glass-like thermal conductivity in ytterbium-doped lanthanum zirconate pyrochlore, 6166, Copyright 2010, with permission from Elsevier.

Furthermore, Ren *et al*. [51] achieved a quasi-eutectoid mixture comprising a $La_2Zr_2O_7$-rich pyrochlore phase and a $Yb_2Zr_2O_7$-rich fluorite phase by introducing La^{3+} and Yb^{3+} ions with considerably disparate atomic radii at the A site. The grain size decreases to 0.8–1 μm, and a considerably low thermal conductivity is attributed to the rattling effect and strong heat-carrying phonon scattering. With a similar phase transition, Wu *et al*. [52] used a solid-state reaction at 1600°C for 10 h to prepare a sequence of $(Nd_{1-x}Yb_x)_2Zr_2O_7$ (x = 0, 0.2, 0.4, 0.6, 0.8, 1.0) ceramics. A pyrochlore–fluorite transformation of $(Nd_{1-x}Yb_x)_2Zr_2O_7$ ceramics was observed when increasing the doping concentration of Yb. Additionally, Guo *et al*. [76] prepared Yb_2O_3 and Sc_2O_3 co-doped $Gd_2Zr_2O_7$

ceramics by chemical coprecipitation. The co-doping of Yb_2O_3 and Sc_2O_3 facilitates the order–disorder transition from the pyrochlore structure to the fluorite structure. Moreover, Sc_2O_3 doping helped enhance fracture toughness in comparison with undoped $Gd_2Zr_2O_7$.

The influence of the rattler effect on thermal conductivity was investigated by Yang *et al*. [77] by synthesizing a sequence of multicomponent ceramics, namely, $(La_{1/3}Eu_{1/3}Gd_{1/3})_{2-2x}Yb_{2x}Zr_2O_7$ (x = 0, 0.25, 0.5, 0.75, and 1). A schematic representation of the rattler effect is shown in Fig. 12. The phase transition from the pyrochlore structure to the fluorite structure was observed with increasing Yb^{3+} content. Dual-phase $(La_{1/3}Eu_{1/3}Gd_{1/3})_{1.5}Yb_{0.5}Zr_2O_7$ ceramics has a high coefficient of thermal expansion of 11.2×10^{-6} K^{-1}. Li *et al*. [78] prepared 6 types of $(Nd_{1/2}Sm_{1/2}Eu_{1/2}Gd_{1/2})_{1-x}Dy_{2x}Zr_2O_7$ rare-earth zirconates using a solid-state reaction. The augmentation of Dy^{3+} incorporation leads to a phase transition from an ordered pyrochlore to a disordered fluorite occurring with increasing Dy^{3+}, thereby providing a descriptor for predicting the formation of a single- or dual-phase system.

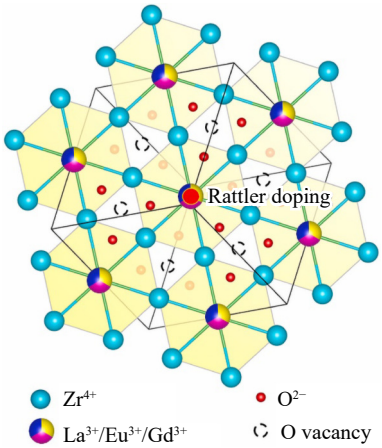

Fig. 12. Schematic of the crystal structure of multicomponent $RE_2Zr_2O_7$ ceramics doped by the rattler effect. Reprinted from *Ceram. Int.*, 48, R. Yang, J. Xu, M. Wei, *et al.*, Rattler effect on the properties of multicomponent rare-earth zirconate ceramics, 28586, Copyright 2022, with permission from Elsevier.

Fan *et al*. [55] used molecular dynamics to calculate the TECs of a sequence of rare earth zirconates. The Zr–O bond is considered the primary determinant of overall TECs, while the A–O bond plays a secondary role and O–O has minimal impact on TECs based on potential functions and equilibrium-location deviations between atoms. Using DFT, Zhao *et al*. [79] investigated the mechanical properties, Debye temperatures, thermal conductivities, and electronic structures of $Gd_{2-x}Th_xZr_2O_7$ and $Gd_2Zr_{2-x}Th_xO_7$ pyrochlores. The Young's modulus, Debye temperature, and thermal conductivity of $Gd_2Zr_{2-x}Th_xO_7$ exhibit generally lower values compared to $Gd_{2-x}Th_xZr_2O_7$, as predicted by Clarke's model. Furthermore, a reduction of thermal conductivity by doping was predicted through a comprehensive computational route proposed by Lan *et al*. [80], which is based on first-principles calculations. Thermodynamic modeling was combined with the first-principles calculations, with clarified defects from doping.

(2) B-site doping.

The introduction of B-site doping in rare earth zirconates, which exhibits excellent chemical and structural compatibility, can also effectively enhance lattice distortion and reduce the phonon mean free path. The selection of B-site elements is limited because of their high coordination and small ionic radius, in contrast to the wider range of choices available for A-site elements. However, the doping of B-site elements enhances the flexibility in tailoring the TEC. According to Liu *et al*. [81], the TEC decreases with increasing Ti content at a given temperature level, which may attributed to the pyrochlore phase of Ti doping ranging from 25mol% to 100mol%. However, the doping of Ti did not increase the TEC as expected. Zhang *et al*. [53] prepared the $Sm_2(Zr_{0.6}Ce_{0.4})_2O_7$ ceramic with a fluorite structure using a solid-state reaction at 1600°C for 10 h. The thermal conductivity of $Sm_2(Zr_{0.6}Ce_{0.4})_2O_7$ is lower than that of YSZ but higher than that of $Sm_2Zr_2O_7$, which can be attributed to the phase transition from pyrochlore to fluorite. The nano-sized $La_2(Zr_{0.7}Ce_{0.3})_2O_7$ ceramic as a novel TBC material was synthesized by Wang *et al*. [82] using the sol–gel process. $La_2(Zr_{0.7}Ce_{0.3})_2O_7$ maintains a pyrochlore-type structure at 1000–1500°C and exhibits exceptional thermal stability through prolonged annealing at 1400°C.

$La_2(Zr_{1-x}Ce_x)_2O_{7-\delta}$ was synthesized by a soft chemistry method [53]. The fluorite-type structure is stable until 1400°C in air and then evolves into pyrochlore- and fluorite-type structures. Wang *et al*. [83] studied the determining factors of substitutional defects on thermal conductivity (k) by doping Hf^{4+} (which is 96% heavier than Zr^{4+} but has a similar ionic radius) and Ce^{4+} (50% heavier and 21% larger), as replacements for Zr^{4+} on the B site of $La_2Zr_2O_7$ pyrochlores (Fig. 13). They found that the size values of the dopants determine k_{min}, which may provide guidelines for low-k material design and selection. Ma *et al*. [84] synthesized the $La_2(Zr_{1-x}Ce_x)_2O_7$ (x = 0, 0.3, 0.5, 1.0) ceramics by the coprecipitation–calcination method and then investigated the mechanical and thermophysical properties of $La_2(Zr_{1-x}Ce_x)_2O_7$. $La_2(Zr_{0.7}Ce_{0.3})_2O_7$ effectively mitigates the abrupt decrease in thermal expansion observed in $La_2Ce_2O_7$ and exhibits a low sintering rate of 1.13×10^{-7} s^{-1} at 1400°C. Cerium was introduced as a substitution for zirconium by Yang *et al*. [54] to enhance the TEC of rare earth zirconates. A sequence of $Yb_2(Zr_{1-x}Ce_x)_2O_7$ was prepared using a solid-state reaction. The increase in TEC with the volume fraction of Ce substitution is ascribed to the lattice relaxation and the conversion of Ce^{4+} to Ce^{3+} at elevated temperature. The thermal conductivity of doped $Yb_2(Zr_{1-x}Ce_x)_2O_7$ is lower than that of pure $Yb_2Zr_2O_7$.

(3) Co-doping at A site and B site.

The excellent structural and chemical stability of $A_2B_2O_7$-type rare earth zirconates makes it feasible to consider co-doping of the A site and B site. Liu *et al*. [85] used the solid-state reaction method to synthesize single phase $(La_{0.4}Sm_{0.5}Yb_{0.1})_2(Zr_{0.7}Ce_{0.4})_2O_{7.4}$ and $(Sr_{0.1}La_{0.3}Sm_{0.5}Yb_{0.1})_2(Zr_{0.7}Ce_{0.4})_2O_{7.3}$ with a pyrochlore structure. The lower

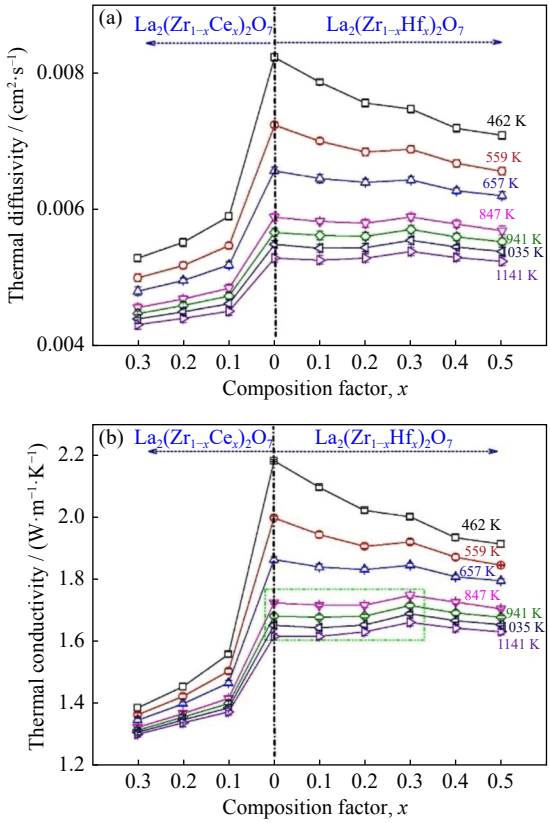

Fig. 13. Plots of (a) thermal diffusivity and (b) thermal conductivity of Hf/Ce-doped $La_2Zr_2O_7$ with the single pyrochlore phase vs. the dopant content x. Reprinted from *Acta Mater.*, 68, Y. Wang, F. Yang, and P. Xiao, Role and determining factor of substitutional defects on thermal conductivity: A study of $La_2(Zr_{1-x}B_x)_2O_7$ (B = Hf and Ce, $0 \le x \le 0.5$) pyrochlore solid solutions, 106, Copyright 2014, with permission from Elsevier.

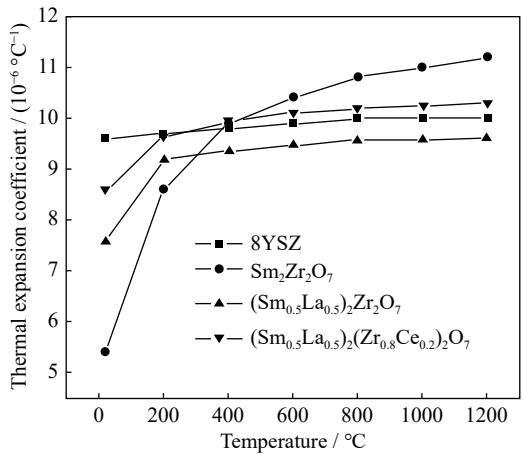

Fig. 14. Linear thermal expansion of $Sm_2Zr_2O_7$, $(Sm_{0.5}La_{0.5})_2Zr_2O_7$, $(Sm_{0.5}La_{0.5})_2(Zr_{0.8}Ce_{0.2})_2O_7$, and 8YSZ. Reprinted from *J. Alloys Compd.*, 475, H.S. Zhang, Q. Xu, F.C. Wang, L. Liu, Y. Wei, and X.G. Chen, Preparation and thermophysical properties of $(Sm_{0.5}La_{0.5})_2Zr_2O_7$ and $(Sm_{0.5}La_{0.5})_2(Zr_{0.8}Ce_{0.2})_2O_7$ ceramics for thermal barrier coatings, 624, Copyright 2009, with permission from Elsevier.

thermal conductivity and slightly higher TEC of $(Sr_{0.1}La_{0.3}Sm_{0.5}Yb_{0.1})_2(Zr_{0.7}Ce_{0.4})_2O_{7.3}$ can be attributed to the difference in atomic weight of the substitutional cation and the increased concentration of oxygen vacancies in this material. Furthermore, Zhang *et al.* [15] synthesized rare earth zirconates $(Sm_{0.5}La_{0.5})_2Zr_2O_7$ and $(Sm_{0.5}La_{0.5})_2(Zr_{0.8}Ce_{0.2})_2O_7$ ceramics with a pyrochlore structure via a solid-state reaction method at 1600°C for 10 h. Because of phonon scattering resulting from doping of La_2O_3 and CeO_2, the $(Sm_{0.5}La_{0.5})_2(Zr_{0.8}Ce_{0.2})_2O_7$ ceramic exhibits low thermal conductivity and high TEC above 400°C, as shown in Fig. 14. Zhou *et al.* [56] investigated the effect of rare earth doping on the thermophysical properties of $La_2Zr_2O_7$ synthesized via the coprecipitation–calcination method. $La_2(Zr_{1.8}Ce_{0.2})_2O_7$ and $La_{1.7}(DyNd)_{0.15}(Zr_{0.8}Ce_{0.2})_2O_7$ with pyrochlore structure have higher TECs than $La_2Zr_2O_7$ and $La_{1.7}Dy_{0.3}Zr_2O_7$. All the doped ceramics have lower thermal conductivity than undoped $La_2Zr_2O_7$.

Liu *et al.* [86] prepared single-phase pyrochlore $(Mg_xLa_{0.5-x}Sm_{0.5})_2(Zr_{0.7}Ce_{0.3})_2O_{7-x}$ (x = 0, 0.1, 0.2, 0.3) using the coprecipitation–calcination method. When doping up to x = 0.2, thermal conductivity has a minimum value near 1.57 W/(m·K), and the TEC reaches a peak of 11.3×10^{-6} K^{-1}. Additionally, Zhao *et al.* [87] prepared dense monoliths with dual-phase rare-earth zirconate–stannate structures of $Yb_2Zr_2O_7 + Ln_2Sn_2O_7$ (Ln = Nd and Sm) using a solid-state reaction. Dual-phase structures of $Yb_2Zr_2O_7$-rich fluorite and $Nd_2Sn_2O_7$-rich pyrochlore were observed in the specimens of $(1-x)Yb_2Zr_2O_7 + xNd_2Sn_2O_7$ (x = 0.4 and 0.5); however, a complete solid solution of $(Yb_{1-x}Sm_x)_2(Zr_{1-x}Sn_x)_2O_7$ was finally formed in the case of sintering the $(1-x)Yb_2Zr_2O_7 + xSm_2Sn_2O_7$ series. In both series, low thermal conductivities with a positive temperature dependence are realized, as shown in Fig. 15. Xue *et al.* [88] prepared a sequence of Y_2O_3 and Ta_2O_5 co-doped $Gd_2Zr_2O_7$, designated as $(Gd_{1-x}Y_x)_2(Zr_{1-x}Ta_x)_2O_{7+x}$ (x = 0, 0.1, 0.2, 0.3, and 0.4), using a solid-state reaction. The measured thermal conductivity of doped $Gd_2Zr_2O_7$ has a minimum of 1.41 W/(m·K) at 800°C and x = 0.3. The phase stability of $(Gd_{0.7}Y_{0.3})_2(Zr_{0.7}Ta_{0.3})_2O_{7.3}$ is illustrated in Fig. 16.

(4) Cationic substitutions in rare earth zirconate ceramic coatings.

Even if numerous voids present in the coating, rare earth zirconate ceramic topcoat can be improved by cationic doping. Guo *et al.* [89] prepared $(Gd_{0.9}Yb_{0.1})_2Zr_2O_7$/YSZ double-layer ceramic TBCs using EB-PVD. The coatings showed more than 3700 thermal cycle lifespan at approximately 1350°C during flame shock test and the lowest thermal conductivity, as shown in Fig. 17. Zhou *et al.* [90] fabricated the $La_2(Zr_{0.75}Ce_{0.25})_2O_7$ coatings by APS using nanostructured feedstocks. These nanostructured $La_2(Zr_{0.75}Ce_{0.25})_2O_7$ coatings exhibit a favorable wear resistance. $Gd_2Zr_2O_7$ coatings doped with Ti^{4+} or Mg^{2+} were fabricated by Wang *et al.* [91]. The incorporation of Ti^{4+} into $Gd_2Zr_2O_7$ can enhance the infrared absorption/emittance within a specific wavenumber range (0.75–2.5 μm), which is due to the augmentation of electronic transitions induced by the impurity energy levels associated with the widening of the conduction band. Shen *et al.* [92] deposited the $(Gd_{0.9}Er_{0.1})_2Zr_2O_7$/YSZ double-layer TBCs by EB-PVD, which exhibits a measured thermal conductivity of 0.95 W/(m·K) at 1000°C and 1.02 W/(m·K) at

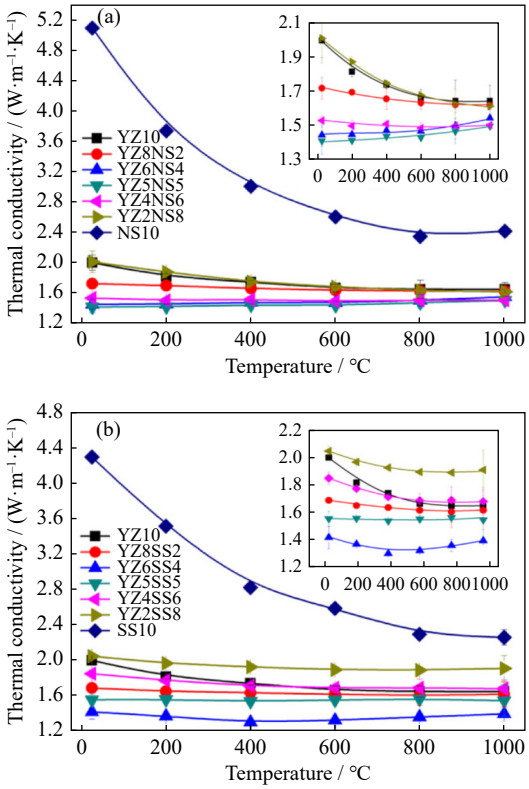

Fig. 15. Thermal conductivity of the specimens: (a) $(1-x)Yb_2Zr_2O_7 + xNd_2Sn_2O_7$ series; (b) $(1-x)Yb_2Zr_2O_7 + xSm_2Sn_2O_7$ series. M. Zhao, X.R. Ren, J. Yang, and W. Pan, *J. Am. Ceram. Soc.*, 99, 293(2016) [87]. Copyright Wiley-VCH Verlag GmbH & Co. KGaA. Reproduced with permission ($YZ10—Yb_2Zr_2O_7$; $YZ8NS2—(Yb_2Zr_2O_7)_{0.8}(Nd_2Sn_2O_7)_{0.2}$; $YZ6NS4—(Yb_2Zr_2O_7)_{0.6}(Nd_2Sn_2O_7)_{0.4}$; $YZ5NS5—(Yb_2Zr_2O_7)_{0.5}(Nd_2Sn_2O_7)_{0.5}$; $YZ4NS6—(Yb_2Zr_2O_7)_{0.4}(Nd_2Sn_2O_7)_{0.6}$; $YZ2NS8—(Yb_2Zr_2O_7)_{0.2}(Nd_2Sn_2O_7)_{0.8}$; $NS10—Nd_2Sn_2O_7$; $YZ8SS2—(Yb_2Zr_2O_7)_{0.8}(Sm_2Sn_2O_7)_{0.2}$; $YZ6SS4—(Yb_2Zr_2O_7)_{0.6}(Sm_2Sn_2O_7)_{0.4}$; $YZ5SS5—(Yb_2Zr_2O_7)_{0.5}(Sm_2Sn_2O_7)_{0.5}$; $YZ4SS6—(Yb_2Zr_2O_7)_{0.4}(Sm_2Sn_2O_7)_{0.6}$; $YZ2SS8—(Yb_2Zr_2O_7)_{0.2}(Sm_2Sn_2O_7)_{0.8}$; $SS10—Sm_2Sn_2O_7$).

1200°C. Additionally, Jiang *et al.* [93] fabricated Y-doped $La_2Zr_2O_7$ coatings with a Y to La molar ratio of 1:1 via the APS method. The fluorite phase begins to precipitate after prolonged annealing, increasing thermal conductivity. The presence of a robust phonon scattering source, in conjunction with the suppression of radiative thermal conduction, constitutes the underlying mechanism for low thermal conductivity.

3.1.3. Design on high-entropy rare earth zirconate ceramics

Since high-entropy alloys (HEAs) were proposed in 2004, the concept of high entropy has attracted increasing attention [94–95]. Ceramic scientists have extended the concept of high entropy into different advanced ceramic materials, including oxides, carbides, borides, nitrides, silicides, carbonitrides, and even composites [25–26]. The term high-entropy ceramics refers to a single-phase system where almost equimolar multicomponent elements not less than five cations occupy the same lattice site, resulting in a considerably large configurational entropy ($S_{conf} \geq 1.5R$, with R representing the ideal gas constant) [25].

Depending on the demand for high-entropy ceramics on a single phase, the formation ability of a single phase becomes an important issue that must be studied [28]. A size disorder parameter has been expanded to high-entropy zirconates to tailor the thermal conductivity [96] and the single-phase formation ability [97]. Yang *et al.* [98] synthesized a five-component equimolar high-entropy ceramic of $(La_{0.2}Eu_{0.2}Gd_{0.2}Y_{0.2}Yb_{0.2})_2Zr_2O_7$ with a dual-phase of pyrochlore and fluorite structures. They claimed that the single-phase forming ability is determined by the difference in cationic radius rather than the entropy, with a critical threshold value of 5.2%. Subsequently, Wang *et al.* [97] prepared a sequence of five-principal equimolar rare earth zirconates via a solid-state reaction method. The single-phase formation ability was mainly controlled by the size disorder parameter (δ*); meanwhile, the average cation radius ratio (r_A/r_B) is the threshold value for the formation of a pyrochlore- or defective fluorite-type structure. When δ* is less than 5%, multicomponent zirconate ceramics tend to form a single phase; otherwise, a dual-phase ceramic with pyrochlore and defective fluorite structures occurs, as shown in Fig. 18. They also concluded that the threshold value of the average cation radius ratio is tailored accurately to be 1.467 for a phase transition of pyro-

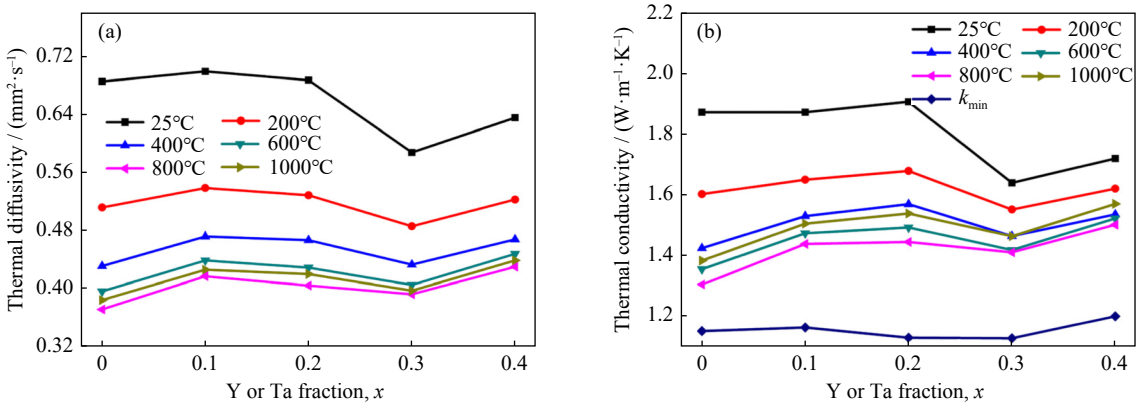

Fig. 16. Thermal diffusivities (a) and thermal conductivities (b) of $(Gd_{1-x}Y_x)_2(Zr_{1-x}Ta_x)_2O_{7+x}$ series ceramics as a function of Y or Ta doping concentration. Reprinted by permission from Springer Nature: *J. Mater. Eng. Perform.*, Influence of Y_2O_3 and Ta_2O_5 co-doping on microstructure and thermal conductivity of $Gd_2Zr_2O_7$ ceramics, Z.L. Xue, S.Q. Wu, L.H. Qian, E. Byon, and S.H. Zhang, Copyright 2020.

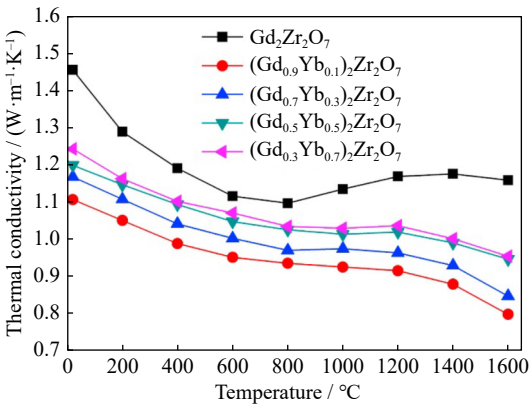

Fig. 17. Thermal conductivity of $(Gd_{1-x}Yb_x)_2Zr_2O_7$ (x = 0, 0.1, 0.3, 0.5, and 0.7) ceramics. Reprinted from *J. Eur. Ceram. Soc.*, 34, L. Guo, H.B. Guo, H. Peng, and S.K. Gong, Thermophysical properties of Yb_2O_3-doped $Gd_2Zr_2O_7$ and thermal cycling durability of $(Gd_{0.9}Yb_{0.1})_2Zr_2O_7$/YSZ thermal barrier coatings, 1255, Copyright 2014, with permission from Elsevier.

chlore to defective fluorite when δ* is less than 5%.

(1) High-entropy single-phase zirconates.

In a strict sense, the term "high-entropy ceramics" should be reserved exclusively for single-phase ceramics. Consequently, many researchers have investigated rare earth composition adjustments to explore single-phase high-entropy rare earth zirconates. Li *et al*. [99] prepared high-entropy pyrochlore-type structures based on rare earth zirconates $(5RE_{1/5})_2Zr_2O_7$ (RE = La, Nd, Sm, Eu, Gd, and Y) via a solid-state reaction method. The measured thermal conductivities of $(5RE_{1/5})_2Zr_2O_7$ high-entropy ceramics are below 1 W/(m·K). Zhao *et al*. [29] synthesized a high-entropy rare-earth zirconate of $(La_{0.2}Ce_{0.2}Nd_{0.2}Sm_{0.2}Eu_{0.2})_2Zr_2O_7$. With a sluggish grain growth rate, the thermal conductivity of $(La_{0.2}Ce_{0.2}Nd_{0.2}Sm_{0.2}Eu_{0.2})_2Zr_2O_7$ is only 0.76 W/(m·K) at room temperature. Furthermore, Ren *et al*. [100] prepared $(Sm_{0.2}Eu_{0.2}Tb_{0.2}Dy_{0.2}Lu_{0.2})_2Zr_2O_7$ and $(Sm_{1/3}Eu_{1/3}Dy_{1/3})_2Zr_2O_7$ by spark plasma sintering. The high-entropy ceramics exhibited an enhanced Young's modulus, and the fracture toughness of the $(Sm_{0.2}Eu_{0.2}Tb_{0.2}Dy_{0.2}Lu_{0.2})_2Zr_2O_7$ bulk ceramic was measured to be approximately 2.24 MPa·m$^{1/2}$, higher than those of single-component $Sm_2Zr_2O_7$ and $Lu_2Zr_2O_7$. The $(Sm_{0.2}Eu_{0.2}Tb_{0.2}Dy_{0.2}Lu_{0.2})_2Zr_2O_7$ ceramic exhibited a low thermal conductivity of 0.86 W/(m·K) and a high TEC of approximately 11 × 10^{-6} K^{-1} at 1000°C. In addition, multicomponent rare-earth cerate $(Sm_{0.2}Eu_{0.2}Tb_{0.2}Dy_{0.2}Lu_{0.2})_2Ce_2O_7$ and zirconocerate $(Sm_{0.2}Eu_{0.2}Tb_{0.2}Dy_{0.2}Lu_{0.2})_2ZrCeO_7$ ceramics synthesized by Ren *et al*. [101] had a homogeneous composition distribution of rare-earth elements and exhibited pure fluorite structure up to 1400°C. The $(Sm_{0.2}Eu_{0.2}Tb_{0.2}Dy_{0.2}Lu_{0.2})_2Ce_2O_7$ ceramic has an improved TEC of 12.60 × 10^{-6} K^{-1} at 1200°C and a reduced thermal conductivity. However, $(Sm_{0.2}Eu_{0.2}Tb_{0.2}Dy_{0.2}Lu_{0.2})_2ZrCeO_7$ zirconocerate exhibited a better sintering resistance than $(Sm_{0.2}Eu_{0.2}Tb_{0.2}Dy_{0.2}Lu_{0.2})_2Ce_2O_7$ cerate.

He *et al*. [102] prepared a sequence of high-entropy ceramics with $RE_2(Ce_{0.2}Zr_{0.2}Hf_{0.2}Sn_{0.2}Ti_{0.2})_2O_7$ ($RE_2HE_2O_7$, RE = Y, Ho, Er, and Yb) compositions using a solid-state reaction. $RE_2HE_2O_7$ ceramics exhibit exceptional phase stability at high temperatures, along with considerably high TECs of 10.3 × 10^{-6}–11.7 × 10^{-6} K^{-1} at 1200°C and low thermal conductivities of 1.10–1.37 W/(m·K) at 25°C, all of which are attributed to the single-phase defective fluorite structure. Subsequently, a $(Y,Yb)_2(Ti,Zr,Hf)_2O_7$ high-entropy ceramic prepared by Song *et al*. [103] has a low glass-like thermal conductivity of 1.27 W/(m·K) at 25°C and a TEC of 10.08 × 10^{-6} K^{-1} at 1000°C, which is attributed to its highly disordered crystal structure and substantial mass disorder among the multiple cations. Zhang *et al*. [104] investigated the structures and thermophysical properties of $(La_{0.2}Gd_{0.2}Y_{0.2}Yb_{0.2}Er_{0.2})_2(Zr_{1-x}Ti_x)_2O_7$ (x = 0 to 0.5) high-entropy ceramics synthesized using a solid-state reaction method. $(La_{0.2}Gd_{0.2}Y_{0.2}Yb_{0.2}Er_{0.2})_2Zr_2O_7$ zirconate shows a defective fluorite structure, and others demonstrate a pure pyrochlore phase. The average coefficients of thermal expansion for $(La_{0.2}Gd_{0.2}Y_{0.2}Yb_{0.2}Er_{0.2})_2(Zr_{1-x}Ti_x)_2O_7$ ceramics range from 10.65 × 10^{-6} to 10.84 × 10^{-6} K^{-1}, while the substitution of Ti^{4+} leads to a reduction in thermal conductivity from 1.66 to 1.20 W/(m·K).

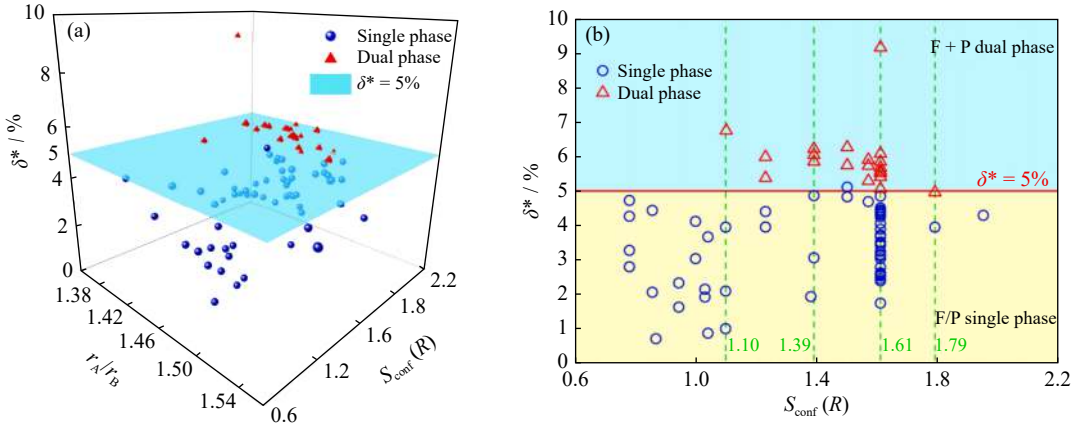

Fig. 18. (a) 3D schematic of the correlation of phase structure with the average ionic radius ratio (r_A/r_B), configuration entropy (S_{conf}), and size disorder (δ*) of the synthesized zirconate ceramics; (b) 2D projection of (a), phase zone distribution dependence on δ* and S_{conf}. Reprinted from *J. Alloys Compd.*, 918, Y.H. Wang, Y.J. Jin, T. Wei, *et al*., Size disorder: A descriptor for predicting single- or dual-phase formation in multicomponent rare earth zirconates, 165636, Copyright 2022, with permission from Elsevier.

In addition, single-phase high-entropy rare-earth zirconate of $(Yb_{0.2}Nd_{0.2}Sm_{0.2}Eu_{0.2}Gd_{0.2})_2Zr_2O_7$ fabricated by Luo *et al*. [105] has a TEC value of 10.52 × 10^{-6} K^{-1} at RT–1500°C and a thermal conductivity of 1.003 W/(m·K). Furthermore, its thermophysical properties are tunable by introducing a high-entropy design to form single-phase rare-earth zirconates utilizing spark plasma sintering [106]. Compared with lanthanum zirconate, the HECs have outstanding high-temperature phase stability, a large TEC of 10.20 × 10^{-6}–10.39 × 10^{-6} K^{-1} at RT–1500°C, low thermal conductivity of 1.17–1.37 W/(m·K) at 1500°C, and fracture toughness of 1.61–1.69 MPa·$m^{1/2}$. Yan *et al*. [107] synthesized a high-entropy $(Gd_{0.2}Y_{0.2}Er_{0.2}Tm_{0.2}Yb_{0.2})_2Zr_2O_7$ zirconate ceramic with a fluorite structure via a solid-state reaction. $(Gd_{0.2}Y_{0.2}Er_{0.2}Tm_{0.2}Yb_{0.2})_2Zr_2O_7$ ceramic has an ultra-low thermal conductivity of 0.82 W/(m·K), a high TEC of 10.61 × 10^{-6} K^{-1}, and a fracture toughness of 1.54 MPa·$m^{1/2}$, which is attributed to the synergistic effects resulting from implementing a high-entropy strategy. Zhang *et al*. [108] investigated the underlying mechanism of unusual thermal conductivity in high-entropy ceramics by synthesizing pure defective fluorite phase $(La_{0.2}Gd_{0.2}Y_{0.2}Yb_{0.2}Er_{0.2})_2(Zr_{1-x}Ce_x)_2O_7$ (x = 0–0.5) high-entropy ceramics using a solid-state reaction method. With increasing CeO_2 content, the effect of electronic thermal conductivity decreases thermal diffusivities and thermal conductivities. Moreover, high-entropy rare earth zirconate powders were deposited as a double-layer ceramic TBC by Zhou *et al*. [109] via APS. The $(La_{0.2}Nd_{0.2}Sm_{0.2}Eu_{0.2}Gd_{0.2})_2Zr_2O_7$ coating exhibited a thermal cycling lifetime of 53 cycles, compared to a lifetime of 10 cycles for the $La_2Zr_2O_7$ system.

(2) High-entropy dual-phase zirconates.

The formation of single-phase ceramics is essential for high-entropy ceramics; however, excessive distortion from the high-entropy strategy often leads to the occurrence of dual-phase ceramics. Zhu *et al*. [110] synthesized a sequence of high-entropy rare earth zirconates with single- and dual-phase structures (Fig. 19). $(La_{0.2}Nd_{0.2}Y_{0.2}Er_{0.2}Yb_{0.2})_2Zr_2O_7$ (LNYEY) with "rattling" ions exhibited a low glass-like thermal conductivity of 1.62–1.59 W/(m·K) at 100–600°C and an enhanced TEC of 10.45 × 10^{-6} K^{-1} at 1000°C. Fan *et al*. [111] prepared a sequence of dual-phase medium- and high-entropy rare earth zirconates by tailoring the principal elements. Dual-phase pyrochlore–fluorite structure formed under the circumstance of an average ionic radius ratio of 1.4 to 1.5 and more than 5% size disorder. Liu *et al*. [112] fabricated high-entropy $Y_2(Ti_{0.2}Zr_{0.2}Hf_{0.2}Nb_{0.2}Ta_{0.2})_2O_7$ and $Y_2(Ti_{0.25}Zr_{0.25}Hf_{0.25}Ta_{0.25})_2O_7$ ceramics via a solid-state reaction, aiming to assess the influence of B-site cations on thermal conductivity. The $Y_2(Ti_{0.2}Zr_{0.2}Hf_{0.2}Nb_{0.2}Ta_{0.2})_2O_7$ ceramic has a thermal conductivity of 1.8 W/(m·K), which is lower than that of $Y_2(Ti_{0.25}Zr_{0.25}Hf_{0.25}Ta_{0.25})_2O_7$ ceramics (1.8 to 2.5 W/(m·K)) at 25 to 1400°C. Wang *et al*. [113] synthesized novel non-equimolar $(Nd_{0.58}Gd_{0.05}Y_{0.05}Er_{0.05}Yb_{0.27})_2Zr_2O_7$ composed of coexisting defect fluorite and pyrochlore phases and $(Nd_{0.2}Gd_{0.2}Y_{0.2}Er_{0.2}Yb_{0.2})_2Zr_2O_7$ by a solid-state reaction. $(Nd_{0.58}Gd_{0.05}Y_{0.05}Er_{0.05}Yb_{0.27})_2Zr_2O_7$ and $(Nd_{0.2}Gd_{0.2}Y_{0.2}Er_{0.2}Yb_{0.2})_2Zr_2O_7$ possess higher TECs and lower thermal conductivities than $Nd_2Zr_2O_7$ (Fig. 20).

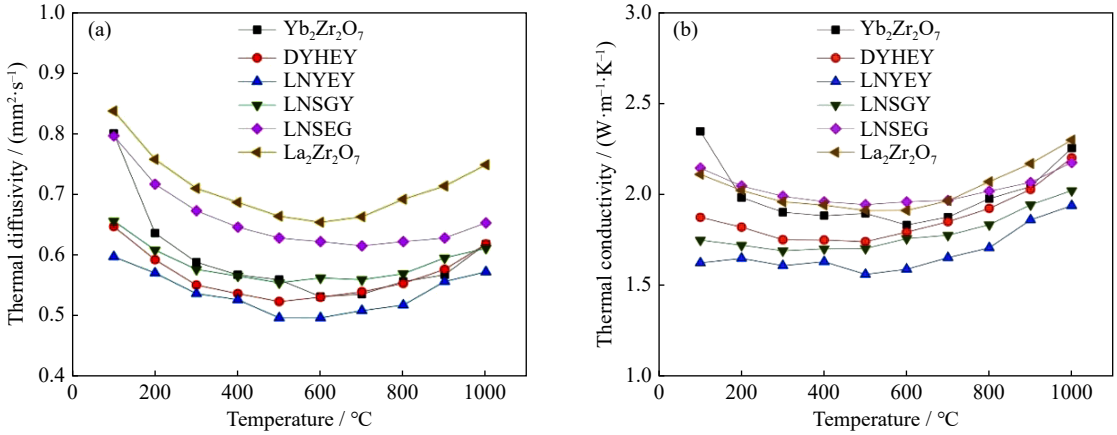

Fig. 19. (a) Thermal diffusivity and (b) thermal conductivity of different $RE_2Zr_2O_7$ ceramics. Reprinted from *J. Eur. Ceram. Soc.*, 41, J.T. Zhu, X.Y. Meng, P. Zhang, *et al*., Dual-phase rare earth zirconate high-entropy ceramics with glass-like thermal conductivity, 2861, Copyright 2021, with permission from Elsevier (LNSEG—$(La_{0.2}Nd_{0.2}Sm_{0.2}Eu_{0.2}Gd_{0.2})_2Zr_2O_7$; LNSGY—$(La_{0.2}Nd_{0.2}Sm_{0.2}Gd_{0.2}Yb_{0.2})_2Zr_2O_7$; LNYEY—$(La_{0.2}Nd_{0.2}Y_{0.2}Er_{0.2}Yb_{0.2})_2Zr_2O_7$; DYHEY—$(Dy_{0.2}Y_{0.2}Ho_{0.2}Er_{0.2}Yb_{0.2})_2Zr_2O_7$; single rare earth $RE_2Zr_2O_7$ (RE = La, Yb)).

(3) Other preparation methods and simulation calculations.

In addition, new theories and techniques have been applied to high-entropy ceramics. Using an innovative high-speed positive grinding strategy combined with a solid-state reaction, Liu *et al*. [114] fabricated high-entropy rare-earth zirconate $(La_{0.2}Nd_{0.2}Sm_{0.2}Gd_{0.2}Yb_{0.2})_2Zr_2O_7$ with a defective fluorite structure, which possesses not only a low thermal conductivity of 0.9–1.72 W/(m·K) at 200–1000°C and a high TEC of 10.9 × 10^{-6} K^{-1} at 1000°C but also excellent mechanical properties, including a high Young's modulus of 186–257 GPa and fracture toughness of 2.7 MPa·$m^{1/2}$. Ultra-fast high-throughput sintering was used to synthesize five lanthanide group rare earth zirconates of $Ln_2Zr_2O_7$ (Ln = La,

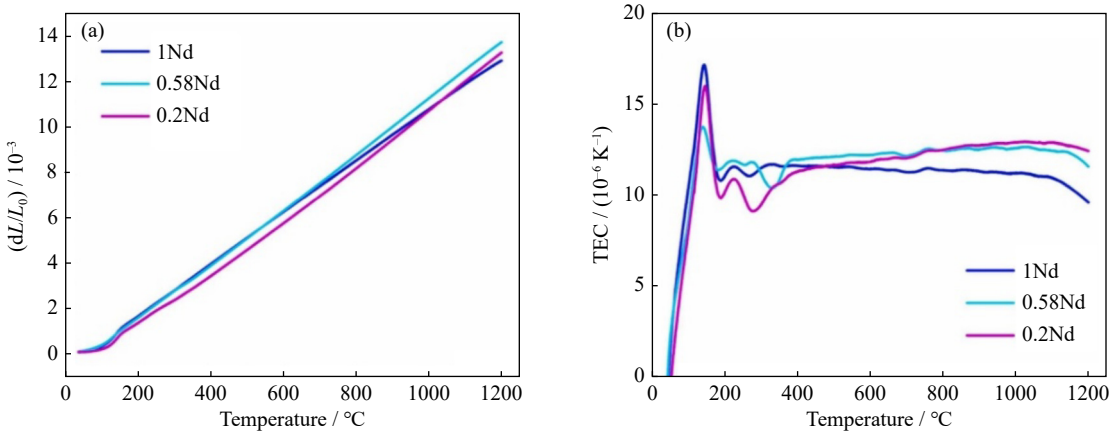

Fig. 20. Relationship between temperature and (a) dL/L_0 and (b) TECs of 1Nd, 0.58Nd, and 0.2Nd samples. Reprinted from *J. Alloys Compd.*, 938, Y.L. Wang, G.Q. Lin, L.X. Yang, *et al.*, Preparation and thermophysical properties of novel dual-phase and single-phase rare earth zirconate high-entropy ceramics, 168551, Copyright 2023, with permission from Elsevier.

Nd, Sm, Eu, and Gd) by Zhao *et al.* [115], as shown in Fig. 21. With an increase in the number of rare earth components, the average grain size of $Ln_2Zr_2O_7$ decreases; however, the hardness and Young's modulus increase, because of the sluggish diffusion and lattice distortion effects caused by an increase in entropy. Using a combustion synthesized nano powder, Zhang *et al.* [116] fabricated a high-entropy ceramic of $(La_{0.2}Nd_{0.2}Sm_{0.2}Gd_{0.2}Yb_{0.2})_2Zr_2O_7$ with a dual-phase of pyrochlore and defective fluorite. The in-line transmittance of the $(La_{0.2}Nd_{0.2}Sm_{0.2}Gd_{0.2}Yb_{0.2})_2Zr_2O_7$ ceramic is 69.06% at a wavelength of 2108 nm. Deng *et al.* [117] synthesized a single-phase high-entropy $(Y_{0.2}Gd_{0.2}Er_{0.2}Yb_{0.2}Lu_{0.2})_2Zr_2O_7$ ceramic by spark plasma sintering, which has a suitable TEC of 10.2 × 10^{-6} K^{-1} and an extremely low thermal conductivity of less than 0.6 W/(m·K) at 25–1000°C. Furthermore, Zhang *et al.* [118] fabricated the high-entropy zirconate of $(La_{0.2}Gd_{0.2}Y_{0.2}Yb_{0.2}Er_{0.2})_2(Zr_{1-x}Ti_x)_2O_7$ to evaluate thermal conductivity at high temperature. For x = 0.1–0.5 compositions, an increased thermal conductivity above 600°C is attributed to the improved photon thermal conductivity.

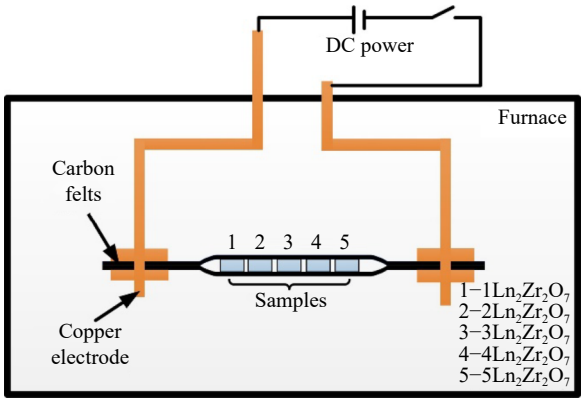

Fig. 21. Schematic of the ultrafast, high-temperature, high-throughput sintering apparatus. Reprinted from *J. Eur. Ceram. Soc.*, 41, Z.T. Zhao, R.F. Guo, H.R. Mao, and P. Shen, Effect of components on the microstructures and properties of rare earth zirconate ceramics prepared by ultrafast high-throughput sintering, 5768, Copyright 2021, with permission from Elsevier.

A first-principles calculation effectively elucidates the effect of ionic bonding and a structural polyhedron on the properties of high-entropy ceramics. Using first-principles calculations, Li *et al.* [119] investigated the influence of chemical disorder on mechanical and thermal properties by producing a pyrochlore-type rare earth zirconate with and without chemical disorder $(nRE_{1/n})_2Zr_2O_7$ (n = 1, 2, and 4, RE = La, Nb, Sm, Eu, and Gd). The lattice parameters of all pyrochlores exhibit a linear increase in RE—O1, RE—O2, and Zr—O2 bonds. Additionally, multicomponent pyrochlores have relatively high elastic constants and moduli. (LaSmEuGd)$_2Zr_2O_7$ has the lowest thermal conductivity. A molecular dynamics simulation is another highly effective computational method. Using molecular dynamics simulations, Fan *et al.* [120] prepared multicomponent rare-earth zirconates $(4RE_{1/4})_2Zr_2O_7$ (RE = La, Nd, Sm, Eu, and Gd) and the corresponding single-component compounds to investigate the temperature-dependent structural and mechanical/thermal property evolution in pyrochlore. With an increase in temperature, the bond lengths increase, and the deformation of (ZrO_6) polyhedra tends to be obvious, which decreases the phonon mean free path and enhances scattering, resulting in lower thermal conductivity.

3.2. Material compositing strategy

To meet the demand for high-temperature infrared radiation resistance and improved mechanical properties, the material compositing strategy has been introduced into TBCs. Li *et al.* [121] investigated the thermal properties of rare earth zirconate composites containing various contents of $NiCr_2O_4$ at elevated temperature. A better general thermal conductivity was achieved with $NiCr_2O_4$ content of 15vol%. The radiative thermal conductivity in $La_2Zr_2O_7$/$LaPO_4$ composites was investigated by Yang *et al.* [122] using a solid-state reaction in air atmosphere. The addition of more than 20wt% $LaPO_4$ was observed to effectively impede radiation thermal conductivity, thereby enhancing fracture toughness. Moreover, Qayyum *et al.* [123] employed DFT to investigate the comprehensive optoelectronic properties of rare-earth

zirconates $Nd_2Zr_2O_7$, encompassing spin-up and spin-down states. They proposed that the calculated optical properties showed a considerable spin-dependent effect. Zhang *et al*. [118] studied the thermal conductivity of the $(La_{0.2}Gd_{0.2}Y_{0.2}Yb_{0.2}Er_{0.2})_2(Zr_{1-x}Ti_x)_2O_7$ high-entropy system. The increase in high-temperature thermal conductivity can be attributed to the effects of improved photon thermal conductivity on actual thermal conductivity. Although the rare earth zirconate exhibits higher transmittance at elevated temperature, it is still better than YSZ TBCs, which was verified by the results of Wang *et al*. [124]. Compared to YSZ, $Gd_2Zr_2O_7$ exhibits enhanced reflectance and reduced transmittance within the wavelength range of 0.8–2.7 μm. Wang *et al*. [125] investigated the heat insulating capacity of multilayer coatings containing a pure $Sm_2Zr_2O_7$ (SZO) layer and a $Sm_2Zr_2O_7$–15vol%$NiCr_2O_4$ (SZO–15%NCO) layer, which exhibited the same insulating capacity (Fig. 22) as the $Sm_2Zr_2O_7$–$NiCr_2O_4$ (SZO–NCO) bulk materials.

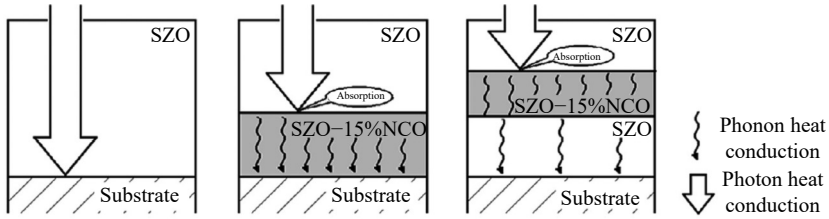

Fig. 22. Schematic for heat conversion in single-, double-, and triple-layer coatings. Reprinted from *Ceram. Int.*, 43, D.Y. Wang, L. Liu, Y.B. Liu, T. Li, Z. Ma, and H.X. Wu, Heat insulating capacity of $Sm_2Zr_2O_7$ coating added with high absorptivity solids, 2884, Copyright 2017, with permission from Elsevier.

Composite ceramics can easily adjust mechanical properties by incorporating different reinforcements. Wang *et al*. [126] added 3mol% Y_2O_3-tetragonal zirconia polycrystals (3Y-TZP) to improve the fracture toughness of $La_2Zr_2O_7$ ceramics. The t-3YSZ/$La_2Zr_2O_7$ composites exhibit a primary toughening mechanism resulting from the phase transformation occurring in dispersive 3YSZ second phases. Zhong *et al*. [127] fabricated $Gd_2Zr_2O_7$ toughened by nanostructured 3mol% yttria-partially stabilized zirconia (YSZ). The $Gd_2Zr_2O_7$–10mol%YSZ composite exhibits a substantial increase in fracture toughness of approximately 60% compared to monolithic $Gd_2Zr_2O_7$. Schmitt *et al*. [128] combined rare earth zirconate $Gd_2Zr_2O_7$ with a thermochemically compatible and phase-stable $GdAlO_3$ aluminate to develop a new strategy. The mechanical properties, particularly fracture toughness, are distinctly enhanced by $GdAlO_3$, and the erosion rate is even reduced by over 61%.

In addition, Luo *et al*. [129] prepared various dual-phase composites $x(5RE)AlO_3/(1-x)(5RE)_2Zr_2O_7$ (x = 0.1–0.5, RE = La, Sm, Eu, Gd, and Yb) using the reverse coprecipitation method. $x(5RE)AlO_3/(1-x)(5RE)_2Zr_2O_7$ have a superior fracture toughness of 2.77 $MPa{\cdot}m^{1/2}$ at x = 0.3, surpassing $Ho_2Zr_2O_7$ by 64% and $La_2Zr_2O_7$ by 101%. Using the reverse coprecipitation method, Yu *et al*. [130] prepared rare earth zirconate/aluminate composites containing Y or Y/Gd, which exhibit a low sintering rate, in contrast to pure fluorite at 1400°C. The rare earth zirconate/aluminate composite containing equimolar Y/Gd exhibits the lowest densification rate at 1500°C. Carpioa *et al*. [131] fabricated multilayered and functionally graded coatings of YSZ/$Gd_2Zr_2O_7$. The multilayered YSZ/$Gd_2Zr_2O_7$ coating exhibited a better thermal fatigue resistance, while the functionally graded YSZ/$Gd_2Zr_2O_7$ coating exhibited an excellent resistance to thermal fatigue. Rai *et al*. [132] prepared a two-phase toughened composite coating containing 30wt% $Gd_2Zr_2O_7$ and 70wt% low-k t'-ZrO_2–2Y_2O_3–1Gd_2O_3–1Yb_2O_3. It is found that erosion performance is improved to address long-term service. Reinforcements of YSZ fibers and multi-walled carbon nanotubes (MWCNTs) were employed by Jin *et al*. [133] to enhance a double-layer YSZ/$La_2Zr_2O_7$ TBC. In contrast to MWCNT-reinforced $La_2Zr_2O_7$ coating, YSZ fibers exhibit the exceptional reinforcement capability of fibers, resulting in considerably reduced thermal conductivity and enhanced bonding strength. In contrast, the $La_2Zr_2O_7$ coating modified with MWCNTs exhibited high fracture toughness and superior thermal cycling stability.

In addition to conventional methods for materials design and research, recent advancements in artificial intelligence have led to the emergence of data-driven scientific approaches that rely on extensive datasets derived from numerous previous experiments and simulations. The use of artificial intelligence (AI), machine learning (ML), deep learning (DL) and big data (BD) techniques has emerged as a crucial driving force in the realm of materials science, facilitating accelerated advancements in materials design and development. The performance of new TBCs can be enhanced from intrinsic and technological perspectives by these future design methods.

To improve the performance of TBCs and promote the development of new TBCs for various industrial applications, the ML and DL models were trained by Liu *et al.* [134] using a substantial amount of YSZ TBC experimental data, revealing that thermal conductivity is considerably influenced by five key factors. Various ML models and algorithms, namely, support vector regression (SVR), Gaussian process regression (GPR), and convolution neural network (CNN) regression algorithms, can considerably enhance the predictive performance of machine learning in estimating thermal conductivity. The effective use of various algorithms and models is observed in the prediction of microstructure features. A support vector machine method optimized by the cuckoo search algorithm (CS-SVM) can filter out the optimal para-

meters of the spray powder size, spray distance, and spray power during APS processing, by which the prediction accuracy has surpassed 95% [135]. In the same pursuit of optimizing the preparation process parameters, Zhu *et al*. [136] employed a typical back propagation (BP) model and extreme machine learning machine (ELM) model combined with the flower pollination algorithm (FPA) optimization algorithm to analyze and train the complex preparation model, which reached 94% accuracy.

4. Conclusions and outlook

In summary, rare earth zirconates have become the most important candidate for applications as TBC materials during the last several decades. Defect engineering, the high-entropy strategy, and compositing approaches have been promising and effective methods for improving the thermophysical properties of rare earth zirconates.

(1) Because of the unique crystal structure of rare earth zirconates, doping emerges as an effective strategy for reducing thermal conductivity and enhancing mechanical properties instead of using vacancies. The impact of lanthanide rare earth ion doping on the basic thermophysical and mechanical properties of zirconate has been extensively investigated through materials design and calculation, with a particular emphasis on the electronic structure of rare earth lanthanides.

(2) Despite the occurrence of component evaporation during coating deposition, high-entropy engineering has garnered considerable attention. Various descriptors have been introduced to characterize phase transitions and the emergence of complex phases resulting from high-entropy designs. A range of computational tools have been employed to explore the mechanism behind the enhancement of properties induced by high-entropy ceramics, which will catalyze future design development in high-entropy strategic materials. However, further investigation is required to explore the impact trends and mechanisms of entropy increase on material properties.

(3) Thermal radiation absorption has gradually become another key point for improving the performance of TBCs, particularly at elevated temperature. The current research in this area is relatively limited, with all studies focusing on incorporating reinforcement phases to create composite materials. Meanwhile, composite strategies are frequently employed to enhance the mechanical properties of rare earth zirconates to achieve a matching thermal expansion with a bond coat.

Doping, high-entropy engineering, and compositing approaches will undoubtedly continue to serve as effective strategies for developing next-generation rare earth zirconate TBC materials characterized by low thermal conductivity, a high thermal expansion match, and superior comprehensive mechanical properties. The heat transfer mechanisms and thermo-optical responses of rare earth zirconates modified with doping, high-entropy engineering, and compositing approaches need in-depth investigation for applications as hot-section components in the advanced turbine engine of the future.

Acknowledgements

The authors would like to thank the financial support from the National Natural Science Foundation of China (Nos. 51572061, 51621091, and 51321061) and the Heilongjiang Touyan Team Program.

Conflict of Interest

Jiahu Ouyang is an editorial board member for this journal and was not involved in the editorial review or the decision to publish this article. The authors declare that they have no known competing financial interests or personal relationships that could have appeared to influence the work reported in this paper.

References

[1] H.F. Chen, C. Zhang, Y.C. Liu, *et al*., Recent progress in thermal/environmental barrier coatings and their corrosion resistance, *Rare Met.*, 39(2020), No. 5, p. 498.

[2] N.P. Padture, M. Gell, and E.H. Jordan, Thermal barrier coatings for gas-turbine engine applications, *Science*, 296(2002), No. 5566, p. 280.

[3] N.P. Padture, Advanced structural ceramics in aerospace propulsion, *Nat. Mater.*, 15(2016), p. 804.

[4] C.G. Levi, J.W. Hutchinson, M.H. Vidal-Sétif, and C.A. Johnson, Environmental degradation of thermal-barrier coatings by molten deposits, *MRS Bull.*, 37(2012), No. 10, p. 932.

[5] D.R. Clarke and C.G. Levi, Materials design for the next generation thermal barrier coatings, *Annu. Rev. Mater. Res.*, 33(2003), p. 383.

[6] Z.G. Liu, W.H. Zhang, J.H. Ouyang, and Y. Zhou, Novel double-ceramic-layer $(La_{0.8}Eu_{0.2})_2Zr_2O_7$/YSZ thermal barrier coatings deposited by plasma spraying, *Ceram. Int.*, 40(2014), No. 7, p. 11277.

[7] Z.G. Liu, W.H. Zhang, J.H. Ouyang, and Y. Zhou, Novel thermal barrier coatings based on rare-earth zirconates/YSZ double-ceramic-layer system deposited by plasma spraying, *J. Alloys Compd.*, 647(2015), p. 438.

[8] U. Schulz, C. Leyens, K. Fritscher, *et al*., Some recent trends in research and technology of advanced thermal barrier coatings, *Aerosp. Sci. Technol.*, 7(2003), No. 1, p. 73.

[9] X.Q. Cao, R. Vassen, and D. Stoever, Ceramic materials for thermal barrier coatings, *J. Eur. Ceram. Soc.*, 24(2004), No. 1, p. 1.

[10] R. Vassen, X.Q. Cao, F. Tietz, D. Basu, and D. Stöver, Zirconates as new materials for thermal barrier coatings, *J. Am. Ceram. Soc.*, 83(2000), No. 8, p. 2023.

[11] M. Zhao, W. Pan, C.L. Wan, Z.X. Qu, Z. Li, and J. Yang, Defect engineering in development of low thermal conductivity materials: A review, *J. Eur. Ceram. Soc.*, 37(2017), No. 1, p. 1.

[12] J. Gild, M. Samiee, J.L. Braun, *et al*., High-entropy fluorite oxides, *J. Eur. Ceram. Soc.*, 38(2018), No. 10, p. 3578.

[13] W.J. Lackey, D.P. Stinton, G.A. Cerny, A.C. Schaffhauser, and L.L. Fehrenbacher, Ceramic coatings for advanced heat engines-A review and projection, *Adv. Ceram. Mater.*, 2(1987), No. 1, p. 24.

[14] C.H. Xu, H.Y. Jin, Q.F. Zhang, *et al*., A novel Co-ions compl-

exation method to synthesize pyrochlore $La_2Zr_2O_7$, *J. Eur. Ceram. Soc.*, 37(2017), No. 8, p. 2871.
[15] H.S. Zhang, Q. Xu, F.C. Wang, L. Liu, Y. Wei, and X.G. Chen, Preparation and thermophysical properties of $(Sm_{0.5}La_{0.5})_2Zr_2O_7$ and $(Sm_{0.5}La_{0.5})_2(Zr_{0.8}Ce_{0.2})_2O_7$ ceramics for thermal barrier coatings, *J. Alloys Compd.*, 475(2009), No. 1-2, p. 624.
[16] N.P. Padture and P.G. Klemens, Low thermal conductivity in garnets, *J. Am. Ceram. Soc.*, 80(1997), No. 4, p. 1018.
[17] C.J. Friedrich, R. Gadow, and M.H. Lischka, Lanthanum hexaaluminate thermal barrier coatings, [in] *25th Annual Conference on Composites, Advanced Ceramics, Materials, and Structures: B: Ceramic Engineering and Science Proceedings*, Florida, 2001, p. 375.
[18] G.W. Schafer and R. Gadow, Lanthane aluminate thermal barrier coating, [in] *23nd Annual Conference on Composites, Advanced Ceramics, Materials, and Structures B: Ceramic Engineering and Science Proceedings*, Hoboken, 1999, p. 291.
[19] L. Chen, M.Y. Hu, P. Wu, and J. Feng, Thermal expansion performance and intrinsic lattice thermal conductivity of ferroelastic $RETaO_4$ ceramics, *J. Am. Ceram. Soc.*, 102(2019), No. 8, p. 4809.
[20] L. Chen, P. Song, and J. Feng, Influence of ZrO_2 alloying effect on the thermophysical properties of fluorite-type Eu_3TaO_7 ceramics, *Scripta Mater.*, 152(2018), p. 117.
[21] J. Yang, W. Pan, Y. Han, M. Zhao, M.Z. Huang, and C.L. Wan, Mechanical properties, oxygen barrier property, and chemical stability of RE_3NbO_7 for thermal barrier coating, *J. Am. Ceram. Soc.*, 103(2020), No. 4, p. 2302.
[22] D.D. Shi, Z.B. Cao, Y.H. Huang, *et al.*, Highly efficient thermal insulation in crystalline weberites RE_3NbO_7 (RE = La, Nd, Sm, Eu, Gd) with glass-like thermal conductivity, *Ceram. Int.*, 48(2022), No. 2, p. 2686.
[23] P.E.D. Morgan and D.B. Marshall, Ceramic composites of monazite and alumina, *J. Am. Ceram. Soc.*, 78(1995), No. 6, p. 1553.
[24] R. Vassen, G. Kerkhoff, and D. Stöver, Development of a micromechanical life prediction model for plasma sprayed thermal barrier coatings, *Mater. Sci. Eng. A*, 303(2001), No. 1-2, p. 100.
[25] S. Akrami, P. Edalati, M. Fuji, and K. Edalati, High-entropy ceramics: Review of principles, production and applications, *Mater. Sci. Eng. R Rep.*, 146(2021), art. No. 100644.
[26] R.Z. Zhang and M.J. Reece, Review of high entropy ceramics: Design, synthesis, structure and properties, *J. Mater. Chem. A*, 7(2019), No. 39, p. 22148.
[27] A.J. Wright and J. Luo, A step forward from high-entropy ceramics to compositionally complex ceramics: A new perspective, *J. Mater. Sci.*, 55(2020), No. 23, p. 9812.
[28] A.J. Wright, Q.Y. Wang, C.Z. Hu, Y.T. Yeh, R.K. Chen, and J. Luo, Single-phase duodenary high-entropy fluorite/pyrochlore oxides with an order-disorder transition, *Acta Mater.*, 211(2021), art. No. 116858.
[29] Z.F. Zhao, H.M. Xiang, F.Z. Dai, Z.J. Peng, and Y.C. Zhou, $(La_{0.2}Ce_{0.2}Nd_{0.2}Sm_{0.2}Eu_{0.2})_2Zr_2O_7$: A novel high-entropy ceramic with low thermal conductivity and sluggish grain growth rate, *J. Mater. Sci. Technol.*, 35(2019), No. 11, p. 2647.
[30] S. Divilov, H. Eckert, D. Hicks, *et al.*, Disordered enthalpy-entropy descriptor for high-entropy ceramics discovery, *Nature*, 625(2024), No. 7993, p. 66.
[31] G. Grimvall, *Thermophysical Properties of Materias*, Elsevier, Amsterdam, 1999.
[32] W.D. Kingery, H.K. Bowen, and D.R. Uhlmann, *Introduction to Ceramics*, John Wiley & Sons, New York, 1976.
[33] M.G. Holland, Analysis of lattice thermal conductivity, *Phys. Rev.*, 132(1963), No. 6, p. 2461.
[34] B. Abeles, Lattice thermal conductivity of disordered semiconductor alloys at high temperatures, *Phys. Rev.*, 131(1963), No. 5, p. 1906.
[35] P.G. Klemens, Thermal resistance due to point defects at high temperatures, *Phys. Rev.*, 119(1960), No. 2, p. 507.
[36] J. Callaway and H.C. von Baeyer, Effect of point imperfections on lattice thermal conductivity, *Phys. Rev.*, 120(1960), No. 4, p. 1149.
[37] X.D. He, Y.B. Li, L.D. Wang, Y. Sun, and S. Zhang, High emissivity coatings for high temperature application: Progress and prospect, *Thin Solid Films*, 517(2009), No. 17, p. 5120.
[38] D.L. Zhao, A. Aili, Y. Zhai, *et al.*, Radiative sky cooling: Fundamental principles, materials, and applications, *Appl. Phys. Rev.*, 6(2019), No. 2, art. No. 021306.
[39] B. Zhao, M.K. Hu, X.Z. Ao, N. Chen, and G. Pei, Radiative cooling: A review of fundamentals, materials, applications, and prospects, *Appl. Energy*, 236(2019), p. 489.
[40] H.Z. Liu, J.H. Ouyang, Z.G. Liu, and Y.M. Wang, Thermo-optical properties of $LaMAl_{11}O_{19}$ (M=Mg, Mn, Fe) hexaaluminates for high-temperature thermal protection applications, *J. Am. Ceram. Soc.*, 94(2011), No. 10, p. 3195.
[41] G.L. Chen, H.Y. Fu, Y.C. Zou, *et al.*, A promising radiation thermal protection coating based on lamellar porous Ca–Cr co-doped Y_3NbO_7 ceramic, *Adv. Funct. Mater.*, 33(2023), No. 47, art. No. 2305650.
[42] S.M. Wang, F.H. Kuang, Q.Z. Yan, C.C. Ge, and L.H. Qi, Crystallization and infrared radiation properties of iron ion doped cordierite glass-ceramics, *J. Alloys Compd.*, 509(2011), No. 6, p. 2819.
[43] K. Krieble, T. Schaeffer, J.A. Paulsen, A.P. Ring, C.C.H. Lo, and J.E. Snyder, Mössbauer spectroscopy investigation of Mn-substituted Co–ferrite ($CoMn_xFe_{2-x}O_4$), *J. Appl. Phys.*, 97(2005), No. 10, art. No. 10F101.
[44] M.A. Subramanian, G. Aravamudan, and G.V.S. Rao, Oxide pyrochlores–A review, *Prog. Solid State Chem.*, 15(1983), No. 2, p. 55.
[45] Z.G. Liu, J.H. Ouyang, and Y. Zhou, Preparation and thermophysical properties of $(Nd_xGd_{1-x})_2Zr_2O_7$ ceramics, *J. Mater. Sci.*, 43(2008), No. 10, p. 3596.
[46] Z.G. Liu, J.H. Ouyang, and Y. Zhou, Structural evolution and thermophysical properties of $(Sm_xGd_{1-x})_2Zr_2O_7$ ($0 \le x \le 1.0$) ceramics, *J. Alloys Compd.*, 472(2009), No. 1-2, p. 319.
[47] Z.G. Liu, J.H. Ouyang, Y. Zhou, J. Li, and X.L. Xia, Influence of ytterbium- and samarium-oxides codoping on structure and thermal conductivity of zirconate ceramics, *J. Eur. Ceram. Soc.*, 29(2009), No. 4, p. 647.
[48] Z.G. Liu, J.H. Ouyang, Y. Zhou, J. Li, and X.L. Xia, Densification, structure, and thermophysical properties of ytterbium–gadolinium zirconate ceramics, *Int. J. Appl. Ceram. Technol.*, 6(2009), No. 4, p. 485.
[49] C.L. Wan, W. Zhang, Y.F. Wang, *et al.*, Glass-like thermal conductivity in ytterbium-doped lanthanum zirconate pyrochlore, *Acta Mater.*, 58(2010), No. 18, p. 6166.
[50] C.L. Wan, Z.X. Qu, A.B. Du, and W. Pan, Order-disorder transition and unconventional thermal conductivities of the $(Sm_{1-x}Yb_x)_2Zr_2O_7$ series, *J. Am. Ceram. Soc.*, 94(2011), No. 2, p. 592.
[51] X.R. Ren, C.L. Wan, M. Zhao, J. Yang, and W. Pan, Mechanical and thermal properties of fine-grained quasi-eutectoid $(La_{1-x}Yb_x)_2Zr_2O_7$ ceramics, *J. Eur. Ceram. Soc.*, 35(2015), No. 11, p. 3145.
[52] Y. Wu, L. Zheng, W.T. He, J. He, and H.B. Guo, Effects of Yb^{3+} doping on phase structure, thermal conductivity and fracture toughness of $(Nd_{1-x}Yb_x)_2Zr_2O_7$, *Ceram. Int.*, 45(2019), No. 3, p. 3133.
[53] H.S. Zhang, K. Sun, Q. Xu, F.C. Wang, and L. Liu, Preparation and thermal conductivity of $Sm_2(Zr_{0.6}Ce_{0.4})_2O_7$ ceramic, *J. Mater. Eng. Perform.*, 18(2009), No. 8, p. 1140.

[54] J. Yang, M. Zhao, L. Zhang, Z.Y. Wang, and W. Pan, Pronounced enhancement of thermal expansion coefficients of rare-earth zirconate by cerium doping, *Scripta Mater.*, 153(2018), p. 1.
[55] Q.B. Fan, F. Zhang, F.C. Wang, and L. Wang, Molecular dynamics calculation of thermal expansion coefficient of a series of rare-earth zirconates, *Comput. Mater. Sci.*, 46(2009), No. 3, p. 716.
[56] H.M. Zhou and D.Q. Yi, Effect of rare earth doping on thermo-physical properties of lanthanum zirconate ceramic for thermal barrier coatings, *J. Rare Earths*, 26(2008), No. 6, p. 770.
[57] J. Wu, X.Z. Wei, N.P. Padture, *et al*., Low-thermal-conductivity rare-earth zirconates for potential thermal-barrier-coating applications, *J. Am. Ceram. Soc.*, 85(2002), No. 12, p. 3031.
[58] Q. Xu, W. Pan, J.D. Wang, *et al*., Preparation and thermophysical properties of $Dy_2Zr_2O_7$ ceramic for thermal barrier coatings, *Mater. Lett.*, 59(2005), No. 22, p. 2804.
[59] Q. Xu, W. Pan, J.D. Wang, *et al*., Rare-earth zirconate ceramics with fluorite structure for thermal barrier coatings, *J. Am. Ceram. Soc.*, 89(2006), No. 1, p. 340.
[60] J. Feng, B. Xiao, R. Zhou, and W. Pan, Thermal conductivity of rare earth zirconate pyrochlore from first principles, *Scr. Mater.*, 68(2013), No. 9, p. 727.
[61] J. Yang, M. Shahid, M. Zhao, J. Feng, C.L. Wan, and W. Pan, Physical properties of $La_2B_2O_7$ (B = Zr, Sn, Hf and Ge) pyrochlore: First-principles calculations, *J. Alloys Compd.*, 663(2016), p. 834.
[62] G.Q. Lan, B. Ouyang, Y.S. Xu, J. Song, and Y. Jiang, Predictions of thermal expansion coefficients of rare-earth zirconate pyrochlores: A quasi-harmonic approximation based on stable phonon modes, *J. Appl. Phys.*, 119(2016), No. 23, art. No. 235103.
[63] X.Q. Wang, X. Bai, W. Xiao, *et al*., Calculation of thermal expansion coefficient of rare earth zirconate system at high temperature by first principles, *Materials*, 15(2022), No. 6, art. No. 2264.
[64] Q. Chen, W. Song, Y. Xie, Z.X. Yan, J. Xu, and F. Gao, Thermal expansion coefficient of nonstoichiometric gadolinium zirconate: First-principles calculations and experimental study, *J. Phys. Chem. Solids*, 178(2023), art. No. 111363.
[65] A. Joulia, M. Vardelle, and S. Rossignol, Synthesis and thermal stability of $Re_2Zr_2O_7$, (Re = La, Gd) and $La_2(Zr_{1-x}Ce_x)_2O_{7-\delta}$ compounds under reducing and oxidant atmospheres for thermal barrier coatings, *J. Eur. Ceram. Soc.*, 33(2013), No. 13-14, p. 2633.
[66] C. Kaliyaperumal, A. Sankarakumar, J. Palanisamy, and T. Paramasivam, Fluorite to pyrochlore phase transformation in nanocrystalline $Nd_2Zr_2O_7$, *Mater. Lett.*, 228(2018), p. 493.
[67] H.B. Zhao, C.G. Levi, and H.N.G. Wadley, Vapor deposited samarium zirconate thermal barrier coatings, *Surf. Coat. Technol.*, 203(2009), No. 20-21, p. 3157.
[68] J.H. Yu, H.Y. Zhao, S.Y. Tao, X.M. Zhou, and C.X. Ding, Thermal conductivity of plasma sprayed $Sm_2Zr_2O_7$ coatings, *J. Eur. Ceram. Soc.*, 30(2010), No. 3, p. 799.
[69] H.B. Zhao, M.R. Begley, A. Heuer, R. Sharghi-Moshtaghin, and H.N.G. Wadley, Reaction, transformation and delamination of samarium zirconate thermal barrier coatings, *Surf. Coat. Technol.*, 205(2011), No. 19, p. 4355.
[70] S.T. Aruna, C. Sanjeeviraja, N. Balaji, and N.T. Manikandanath, Properties of plasma sprayed $La_2Zr_2O_7$ coating fabricated from powder synthesized by a single-step solution combustion method, *Surf. Coat. Technol.*, 219(2013), p. 131.
[71] C. Jiang, E.H. Jordan, A.B. Harris, M. Gell, and J. Roth, Double-layer gadolinium zirconate/yttria-stabilized zirconia thermal barrier coatings deposited by the solution precursor plasma spray process, *J. Therm. Spray Technol.*, 24(2015), No. 6, p. 895.
[72] S. Mahade, N. Curry, S. Björklund, N. Markocsan, and P. Nylén, Thermal conductivity and thermal cyclic fatigue of multilayered $Gd_2Zr_2O_7$/YSZ thermal barrier coatings processed by suspension plasma spray, *Surf. Coat. Technol.*, 283(2015), p. 329.
[73] M. Martena, D. Botto, P. Fino, S. Sabbadini, M.M. Gola, and C. Badini, Modelling of TBC system failure: Stress distribution as a function of TGO thickness and thermal expansion mismatch, *Eng. Fail. Anal.*, 13(2006), No. 3, p. 409.
[74] H. Lehmann, D. Pitzer, G. Pracht, R. Vassen, and D. Stöver, Thermal conductivity and thermal expansion coefficients of the lanthanum rare-earth-element zirconate system, *J. Am. Ceram. Soc.*, 86(2003), No. 8, p. 1338.
[75] Z.G. Liu, J.H. Ouyang, B.H. Wang, Y. Zhou, and J. Li, Preparation and thermophysical properties of $Nd_xZr_{1-x}O_{2-x/2}$ (x = 0.1, 0.2, 0.3, 0.4, 0.5) ceramics, *J. Alloys Compd.*, 466(2008), No. 1-2, p. 39.
[76] Y.Q. Guo, W.T. He, and H.B. Guo, Thermo-physical and mechanical properties of Yb_2O_3 and Sc_2O_3 co-doped $Gd_2Zr_2O_7$ ceramics, *Ceram. Int.*, 46(2020), No. 11, p. 18888.
[77] R.W. Yang, J. Xu, M.Y. Wei, *et al*., Rattler effect on the properties of multicomponent rare-earth-zirconate ceramics, *Ceram. Int.*, 48(2022), No. 19, p. 28586.
[78] M.Y. Li, C.C. Lin, Y.R. Niu, J.M. Zhang, Y. Zeng, and X.M. Song, Order–disorder transition and thermal conductivities of the $(NdSmEuGd)_{(1-x)/2}Dy_{2x}Zr_2O_7$ series, *J. Materiomics*, 9(2023), No. 1, p. 138.
[79] F.A. Zhao, H.Y. Xiao, Z.J. Liu, S.A. Li, and X.T. Zu, A DFT study of mechanical properties, thermal conductivity and electronic structures of Th-doped $Gd_2Zr_2O_7$, *Acta Mater.*, 121(2016), p. 299.
[80] G. Lan, P.F. Ou, C. Chen, and J. Song, A complete computational route to predict reduction of thermal conductivities of complex oxide ceramics by doping: A case study of $La_2Zr_2O_7$, *J. Alloys Compd.*, 826(2020), art. No. 154224.
[81] Z.G. Liu, J.H. Ouyang, Y. Zhou, and X.L. Xia, Effect of Ti substitution for Zr on the thermal expansion property of fluorite-type $Gd_2Zr_2O_7$, *Mater. Des.*, 30(2009), No. 9, p. 3784.
[82] C.J. Wang, Y. Wang, X.Z. Fan, W.Z. Huang, B.L. Zou, and X.Q. Cao, Preparation and thermophysical properties of $La_2(Zr_{0.7}Ce_{0.3})_2O_7$ ceramic via sol–gel process, *Surf. Coat. Technol.*, 212(2012), p. 88.
[83] Y.F. Wang, F. Yang, and P. Xiao, Role and determining factor of substitutional defects on thermal conductivity: A study of $La_2(Zr_{1-x}B_x)_2O_7$ (B = Hf, Ce, $0 \le x \le 0.5$) pyrochlore solid solutions, *Acta Mater.*, 68(2014), p. 106.
[84] W. Ma, X.Y. Li, Y.C. Yin, *et al*., The mechanical and thermophysical properties of $La_2(Zr_{1-x}Ce_x)_2O_7$ ceramics, *J. Alloys Compd.*, 660(2016), p. 85.
[85] L. Liu, Q. Xu, F.C. Wang, and H.S. Zhang, Thermophysical properties of complex rare-earth zirconate ceramic for thermal barrier coatings, *J. Am. Ceram. Soc.*, 91(2008), No. 7, p. 2398.
[86] L. Liu, F.C. Wang, Z. Ma, Q. Xu, and S.G. Fang, Thermophysical properties of $(Mg_xLa_{0.5-x}Sm_{0.5})_2(Zr_{0.7}Ce_{0.3})_2O_{7-x}$ (x = 0, 0.1, 0.2, 0.3) ceramic for thermal barrier coatings, *J. Am. Ceram. Soc.*, 94(2011), No. 3, p. 675.
[87] M. Zhao, X.R. Ren, J. Yang, and W. Pan, Low thermal conductivity of rare-earth zirconate-stannate solid solutions $(Yb_2Zr_2O_7)_{1-x}(Ln_2Sn_2O_7)_x$ (Ln = Nd, Sm), *J. Am. Ceram. Soc.*, 99(2016), No. 1, p. 293.
[88] Z.L. Xue, S.Q. Wu, L.H. Qian, E. Byon, and S.H. Zhang, Influence of Y_2O_3 and Ta_2O_5 co-doping on microstructure and thermal conductivity of $Gd_2Zr_2O_7$ ceramics, *J. Mater. Eng. Perform.*, 29(2020), No. 2, p. 1206.
[89] L. Guo, H.B. Guo, H. Peng, and S.K. Gong, Thermophysical properties of Yb_2O_3 doped $Gd_2Zr_2O_7$ and thermal cycling dur-

ability of $(Gd_{0.9}Yb_{0.1})_2Zr_2O_7$/YSZ thermal barrier coatings, *J. Eur. Ceram. Soc.*, 34(2014), No. 5, p. 1255.

[90] F.F. Zhou, L.P. Xu, C.M. Deng, *et al*., Nanomechanical characterization of nanostructured $La_2(Zr_{0.75}Ce_{0.25})_2O_7$ thermal barrier coatings by nanoindentation, *Appl. Surf. Sci.*, 505(2020), art. No. 144585.

[91] D.Z. Wang, S.J. Dong, J.Y. Zeng, *et al*., Influence of doping Mg^{2+} or Ti^{4+} captions on the microstructures, thermal radiation and thermal cycling behavior of plasma-sprayed $Gd_2Zr_2O_7$ coatings, *Ceram. Int.*, 46(2020), No. 9, p. 13054.

[92] Z.Y. Shen, G.X. Liu, R.D. Mu, L.M. He, Z.H. Xu, and J.W. Dai, Effects of Er stabilization on thermal property and failure behavior of $Gd_2Zr_2O_7$ thermal barrier coatings, *Corros. Sci.*, 185(2021), art. No. 109418.

[93] D. Jiang, Y.F. Wang, S. Wang, R.J. Liu, and J. Han, Thermal conductivity of air plasma sprayed yttrium heavily-doped lanthanum zirconate thermal barrier coatings, *Ceram. Int.*, 45(2019), No. 3, p. 3199.

[94] B. Cantor, I.T.H. Chang, P. Knight, and A.J.B. Vincent, Microstructural development in equiatomic multicomponent alloys, *Mater. Sci. Eng. A*, 375-377(2004), p. 213.

[95] J.W. Yeh, S.K. Chen, S.J. Lin, *et al*., Nanostructured high-entropy alloys with multiple principal elements: Novel alloy design concepts and outcomes, *Adv. Eng. Mater.*, 6(2004), No. 5, p. 299.

[96] A.J. Wright, Q.Y. Wang, S.T. Ko, K.M. Chung, R.K. Chen, and J. Luo, Size disorder as a descriptor for predicting reduced thermal conductivity in medium- and high-entropy pyrochlore oxides, *Scripta Mater.*, 181(2020), p. 76.

[97] Y.H. Wang, Y.J. Jin, T. Wei, *et al*., Size disorder: A descriptor for predicting the single- or dual-phase formation in multi-component rare earth zirconates, *J. Alloys Compd.*, 918(2022), art. No. 165636.

[98] H.B. Yang, G.Q. Lin, H.P. Bu, *et al*., Single-phase forming ability of high-entropy ceramics from a size disorder perspective: A case study of $(La_{0.2}Eu_{0.2}Gd_{0.2}Y_{0.2}Yb_{0.2})_2Zr_2O_7$, *Ceram. Int.*, 48(2022), No. 5, p. 6956.

[99] F. Li, L. Zhou, J.X. Liu, Y.C. Liang, and G.J. Zhang, High-entropy pyrochlores with low thermal conductivity for thermal barrier coating materials, *J. Adv. Ceram.*, 8(2019), No. 4, p. 576.

[100] K. Ren, Q.K. Wang, G. Shao, X.F. Zhao, and Y.G. Wang, Multicomponent high-entropy zirconates with comprehensive properties for advanced thermal barrier coating, *Scripta Mater.*, 178(2020), p. 382.

[101] K. Ren, Q.K. Wang, Y.J. Cao, G. Shao, and Y.G. Wang, Multicomponent rare-earth cerate and zirconocerate ceramics for thermal barrier coating materials, *J. Eur. Ceram. Soc.*, 41(2021), No. 2, p. 1720.

[102] J.J. He, G. He, J. Liu, and J.C. Tao, New class of high-entropy defect fluorite oxides $RE2(Ce_{0.2}Zr_{0.2}Hf_{0.2}Sn_{0.2}Ti_{0.2})_2O_7$ (RE = Y, Ho, Er, or Yb) as promising thermal barrier coatings, *J. Eur. Ceram. Soc.*, 41(2021), No. 12, p. 6080.

[103] D. Song, T. Song, U. Paik, *et al*., Glass-like thermal conductivity in mass-disordered high-entropy $(Y, Yb)_2(Ti, Zr, Hf)_2O_7$ for thermal barrier material, *Mater. Des.*, 210(2021), art. No. 110059.

[104] Y.H. Zhang, M. Xie, Z.G. Wang, *et al*., Marked reduction in the thermal conductivity of $(La_{0.2}Gd_{0.2}Y_{0.2}Yb_{0.2}Er_{0.2})_2Zr_2O_7$ high-entropy ceramics by substituting Zr^{4+} with Ti^{4+}, *Ceram. Int.*, 48(2022), No. 7, p. 9602.

[105] X.W. Luo, L.R. Luo, X.F. Zhao, *et al*., Single-phase rare-earth high-entropy zirconates with superior thermal and mechanical properties, *J. Eur. Ceram. Soc.*, 42(2022), No. 5, p. 2391.

[106] X.W. Luo, R.Q. Huang, C.H. Xu, S. Huang, S.E. Hou, and H.Y. Jin, Designing high-entropy rare-earth zirconates with tunable thermophysical properties for thermal barrier coatings, *J. Alloys Compd.*, 926(2022), art. No. 166714.

[107] R.X. Yan, W.P. Liang, Q. Miao, *et al*., Mechanical, thermal and CMAS resistance properties of high-entropy $(Gd_{0.2}Y_{0.2}Er_{0.2}Tm_{0.2}Yb_{0.2})_2Zr_2O_7$ ceramics, *Ceram. Int.*, 49(2023), No. 12, p. 20729.

[108] Y.H. Zhang, M. Xie, Z.G. Wang, *et al*., Unveiling the underlying mechanism of unusual thermal conductivity behavior in multicomponent high-entropy $(La_{0.2}Gd_{0.2}Y_{0.2}Yb_{0.2}Er_{0.2})_2(Zr_{1-x}Ce_x)_2O_7$ ceramics, *J. Alloys Compd.*, 958(2023), art. No. 170471.

[109] L. Zhou, F. Li, J.X. Liu, *et al*., High-entropy thermal barrier coating of rare-earth zirconate: A case study on $(La_{0.2}Nd_{0.2}Sm_{0.2}Eu_{0.2}Gd_{0.2})_2Zr_2O_7$ prepared by atmospheric plasma spraying, *J. Eur. Ceram. Soc.*, 40(2020), No. 15, p. 5731.

[110] J.T. Zhu, X.Y. Meng, P. Zhang, *et al*., Dual-phase rare-earth-zirconate high-entropy ceramics with glass-like thermal conductivity, *J. Eur. Ceram. Soc.*, 41(2021), No. 4, p. 2861.

[111] W. Fan, Y. Bai, Y.F. Liu, *et al*., Principal element design of pyrochlore-fluorite dual-phase medium- and high-entropy ceramics, *J. Mater. Sci. Technol.*, 107(2022), p. 149.

[112] H.L. Liu, S. Pang, C.Q. Liu, Y.T. Wu, and G.J. Zhang, High-entropy yttrium pyrochlore ceramics with glass-like thermal conductivity for thermal barrier coating application, *J. Am. Ceram. Soc.*, 105(2022), No. 10, p. 6437.

[113] Y.L. Wang, G.Q. Lin, L.X. Yang, *et al*., Preparation and thermophysical properties of a novel dual-phase and single-phase rare-earth-zirconate high-entropy ceramics, *J. Alloys Compd.*, 938(2023), art. No. 168551.

[114] D.B. Liu, B.L. Shi, L.Y. Geng, Y.G. Wang, B.S. Xu, and Y.F. Chen, High-entropy rare-earth zirconate ceramics with low thermal conductivity for advanced thermal-barrier coatings, *J. Adv. Ceram.*, 11(2022), No. 6, p. 961.

[115] Z.T. Zhao, R.F. Guo, H.R. Mao, and P. Shen, Effect of components on the microstructures and properties of rare-earth zirconate ceramics prepared by ultrafast high-throughput sintering, *J. Eur. Ceram. Soc.*, 41(2021), No. 11, p. 5768.

[116] K.B. Zhang, W.W. Li, J.J. Zeng, *et al*., Preparation of $(La_{0.2}Nd_{0.2}Sm_{0.2}Gd_{0.2}Yb_{0.2})_2Zr_2O_7$ high-entropy transparent ceramic using combustion synthesized nanopowder, *J. Alloys Compd.*, 817(2020), art. No. 153328.

[117] S.X. Deng, G. He, Z.C. Yang, J.X. Wang, J.T. Li, and L. Jiang, Calcium–magnesium–alumina–silicate (CMAS) resistant high entropy ceramic $(Y_{0.2}Gd_{0.2}Er_{0.2}Yb_{0.2}Lu_{0.2})_2Zr_2O_7$ for thermal barrier coatings, *J. Mater. Sci. Technol.*, 107(2022), p. 259.

[118] Y.H. Zhang, M. Xie, Z.G. Wang, *et al*., Exploring the increasing behavior of thermal conductivity for high-entropy zirconates at high temperatures, *Scripta Mater.*, 228(2023), art. No. 115328.

[119] Y.R. Li, Q. Wu, M.L. Lai, *et al*., Influence of chemical disorder on mechanical and thermal properties of multi-component rare earth zirconate pyrochlores $(nRE_{1/n})_2Zr_2O_7$, *J. Appl. Phys.*, 132(2022), No. 7, art. No. 075108.

[120] Y. Fan, Q. Wu, Y. Yao, J.M. Wang, J.L. Zhao, and B. Liu, Temperature effect on mechanical and thermal properties of multicomponent rare-earth zirconate pyrochlores, *J. Am. Ceram. Soc.*, 106(2023), No. 2, p. 1500.

[121] T. Li, Z. Ma, L. Liu, and S.Z. Zhu, Thermal properties of $Sm_2Zr_2O_7$–$NiCr_2O_4$ composites, *Ceram. Int.*, 40(2014), No. 7, p. 11423.

[122] J. Yang, C.L. Wan, M. Zhao, M. Shahid, and W. Pan, Effective blocking of radiative thermal conductivity in $La_2Zr_2O_7/LaPO_4$ composites for high temperature thermal insulation applications, *J. Eur. Ceram. Soc.*, 36(2016), No. 15, p. 3809.

[123] A. Qayyum, S. Azam, A.H. Reshak, *et al*., Spin-dependent first-principles study on optoelectronic properties of neodymi-

um zirconates pyrochlores $Nd_2Zr_2O_7$ in Fd-3m and pmma phases, *Molecules*, 27(2022), No. 17, art. No. 5711.

[124] L. Wang, J.I. Eldridge, and S.M. Guo, Thermal radiation properties of plasma-sprayed $Gd_2Zr_2O_7$ thermal barrier coatings, *Scripta Mater.*, 69(2013), No. 9, p. 674.

[125] D.Y. Wang, L. Liu, Y.B. Liu, T. Li, Z. Ma, and H.X. Wu, Heat insulating capacity of $Sm_2Zr_2O_7$ coating added with high absorptivity solids, *Ceram. Int.*, 43(2017), No. 2, p. 2884.

[126] Y.F. Wang and P. Xiao, The phase stability and toughening effect of 3Y-TZP dispersed in the lanthanum zirconate ceramics, *Mater. Sci. Eng. A*, 604(2014), p. 34.

[127] X.H. Zhong, H.Y. Zhao, C.G. Liu, *et al*., Improvement in thermal shock resistance of gadolinium zirconate coating by addition of nanostructured yttria partially-stabilized zirconia, *Ceram. Int.*, 41(2015), No. 6, p. 7318.

[128] M.P. Schmitt, J.L. Stokes, A.K. Rai, A.J. Schwartz, and D.E. Wolfe, Durable aluminate toughened zirconate composite thermal barrier coating (TBC) materials for high temperature operation, *J. Am. Ceram. Soc.*, 102(2019), No. 8, p. 4781.

[129] X.W. Luo, S. Huang, C.H. Xu, S.E. Hou, and H.Y. Jin, Rare-earth high-entropy aluminate-toughened-zirconate dual-phase composite ceramics for advanced thermal barrier coatings, *Ceram. Int.*, 49(2023), No. 1, p. 766.

[130] Y.C. Yu, E.P. Godbole, J. Berrios, N. Hewage, and D.L. Poerschke, Slow sintering in garnet-containing Y and Gd zirconate–aluminate mixtures for thermal barrier coatings, *J. Am. Ceram. Soc.*, 106(2023), No. 8, p. 4519.

[131] P. Carpio, M.D. Salvador, A. Borrell, and E. Sánchez, Thermal behaviour of multilayer and functionally-graded YSZ/$Gd_2Zr_2O_7$ coatings, *Ceram. Int.*, 43(2017), No. 5, p. 4048.

[132] A.K. Rai, M.P. Schmitt, M.R. Dorfman, D.M. Zhu, and D.E. Wolfe, Comparison of single-phase and two-phase composite thermal barrier coatings with equal total rare-earth content, *J. Therm. Spray Technol.*, 27(2018), No. 4, p. 556.

[133] G. Jin, Y.C. Fang, X.F. Cui, *et al*., Effect of YSZ fibers and carbon nanotubes on bonding strength and thermal cycling lifetime of YSZ–$La_2Zr_2O_7$ thermal barrier coatings, *Surf. Coat. Technol.*, 397(2020), art. No. 125986.

[134] Y. Liu, K.Y. Chen, A. Kumar, and P. Patnaik, Principles of machine learning and its application to thermal barrier coatings, *Coatings*, 13(2023), No. 7, art. No. 1140.

[135] D.D. Ye, W.Z. Wang, Z. Xu, C.D. Yin, H.T. Zhou, and Y.J. Li, Prediction of thermal barrier coatings microstructural features based on support vector machine optimized by cuckoo search algorithm, *Coatings*, 10(2020), No. 7, art. No. 704.

[136] H. Zhu, D.P. Li, M. Yang, and D.D. Ye, Prediction of microstructure and mechanical properties of atmospheric plasma-sprayed 8YSZ thermal barrier coatings using hybrid machine learning approaches, *Coatings*, 13(2023), No. 3, art. No. 602.